Received: 7 June 2023 | Revised: 1 February 2024 | Accepted: 4 February 2024

DOI: 10.1002/cac2.12525

CANCER COMMUNICATIONS Open Access

ORIGINAL ARTICLE

Targeting autophagy overcomes cancer-intrinsic resistance to CAR-T immunotherapy in B-cell malignancies

Lu Tang[1,2,3,†] | **Huan Zhang**[4,†] | **Fen Zhou**[5] | **Qiuzhe Wei**[1,2,3] | **Mengyi Du**[1,2,3] | **Jianghua Wu**[1,2,3] | **Chenggong Li**[1,2,3] | **Wenjing Luo**[1,2,3] | **Jie Zhou**[1,2,3] | **Xindi Wang**[1,2,3] | **Zhaozhao Chen**[1,2,3] | **Yinqiang Zhang**[1,2,3] | **Zhongpei Huang**[1,2,3] | **Zhuolin Wu**[1,2,3] | **Yuxi Wen**[5] | **Huiwen Jiang**[1,2,3] | **Danying Liao**[1,2,3] | **Haiming Kou**[1,2,3] | **Wei Xiong**[2] | **Heng Mei**[1,2,3,6] | **Yu Hu**[1,2,3]

[1]Institute of Hematology, Union Hospital, Tongji Medical College, Huazhong University of Science and Technology, Wuhan, Hubei, P. R. China

[2]Hubei Clinical Medical Center of Cell Therapy For Neoplastic Disease, Wuhan, Hubei, P. R. China

[3]Key Laboratory of Biological Targeted Therapy, the Ministry of Education, Wuhan, Hubei, P. R. China

[4]Department of Thoracic Surgery, Union Hospital, Tongji Medical College, Huazhong University of Science and Technology, Wuhan, Hubei, P. R. China

[5]Department of Pediatrics, Union Hospital, Tongji Medical College, Huazhong University of Science and Technology, Wuhan, Hubei, P. R. China

[6]Hubei Key Laboratory of Biological Targeted Therapy, Union Hospital, Tongji Medical College, Huazhong University of Science and Technology, Wuhan, Hubei, P. R. China

Correspondence
Dr. Yu Hu and Dr. Heng Mei, Institute of Hematology, Union Hospital, Tongji Medical College, Huazhong University of Science and Technology, No.1277 Jiefang Avenue, Wuhan 430022, Hubei, P. R. China.
Email: dr_huyu@126.com and hmei@hust.edu.cn

Abstract

Background: Chimeric antigen receptor T (CAR-T) therapy has substantially revolutionized the clinical outcomes of patients with hematologic malignancies, but the cancer-intrinsic mechanisms underlying resistance to CAR-T cells remain yet to be fully understood. This study aims to explore the molecular determinants of cancer cell sensitivity to CAR-T cell-mediated killing and to provide

Abbreviations: APCs, antigen-processing cells; B-ALL, B-cell acute lymphoblastic leukemia; BCMA, B-cell maturation antigen; BLI, bioluminescence imaging; CAR-T, chimeric antigen receptor T; CR, complete remission; CRISPR, clustered regularly interspaced short palindromic repeat; CTLs, cytotoxic T lymphocytes; ChIP, Chromatin immunoprecipitation; Tc, cytotoxic T; CXCL, CXC chemokine ligand; DLBCL, diffuse large B-cell lymphoma; DMEM, Dulbecco's Modified Eagle's Medium; DC, dendritic cell; E:T, effector:target; ECL, enhanced chemiluminescence; FDA, Food and Drug Administration; GSEA, gene set enrichment analysis; IHC, immunohistochemistry; i.p., intraperitoneal injection; i.h., hypodermic injection; i.v., intravenous injection; IRF, interferon regulatory factor; KEGG, Kyoto Encyclopedia of Genes and Genomes; luc, luciferase; MCL, mantle cell lymphoma; MM, multiple myeloma; MOI, multiplicity of infection; MACS, magnetic-activated absorption cell sorting; MIQE, Minimum Information for Publication of Quantitative Real-Time PCR Experiments; MHC-I, major histocompatibility complex I; MDSCs, myeloid-derived suppressor cells; NGS, next-generation sequencing; NK, natural killer; NKT, natural killer T; ns, not significant; PBS, phosphate buffer solution; PCR, polymerase chain reaction; PBS, phosphate-buffered saline; R/R, relapsed/refractory; RRA, robust rank aggregation; RPMI, Roswell Park Memorial Institute; RT-qPCR, real-time quantitative polymerase chain reaction; rpm, revolutions per minute; ROC, receiver operating characteristic; RIPA, radio immunoprecipitation assay; ROI, region of Interest; shRNA, short hairpin RNA; sgRNA, single guide RNA; sgRNA, single-guide RNA; STAT, signal transducers and activators of transcription; TNF, tumor necrosis factor; Tregs, regulatory T cells; Th, T helper; 7-AAD, 7-aminoactinomycin D.

†The authors contributed equally to this article.

Funding information
National Key R&D Program of China, Grant/Award Number: 2022YFC2502700; National Natural Science Foundation of China, Grant/Award Numbers: 81873434, 82100190, 82200145; China Postdoctoral Innovative Talent Support Foundation, Grant/Award Number: BX2021106

a better understanding of the underlying mechanisms and potential modulation to improve clinical efficacy.

Methods: The human whole-genome CRISPR/Cas9-based knockout screening was conducted to identify key genes that enable cancer cells to evade CD19 CAR-T-cell-mediated killing. The in vitro cytotoxicity assays and evaluation of tumor tissue and bone marrow specimens were further conducted to confirm the role of the key genes in cancer cell susceptibility to CAR-T cells. In addition, the specific mechanisms influencing CAR-T cell-mediated cancer clearance were elucidated in mouse and cellular models.

Results: The CRISPR/Cas9-based knockout screening showed that the enrichment of autophagy-related genes (*ATG3*, *BECN1*, and *RB1CC1*) provided protection of cancer cells from CD19 CAR-T cell-mediated cytotoxicity. These findings were further validated by in vitro cytotoxicity assays in cells with genetic and pharmacological inhibition of autophagy. Notably, higher expression of the three autophagy-related proteins in tumor samples was correlated with poorer responsiveness and worse survival in patients with relapsed/refractory B-cell lymphoma after CD19 CAR-T therapy. Bulk RNA sequencing analysis of bone marrow samples from B-cell leukemia patients also suggested the clinical relevance of autophagy to the therapeutic response and relapse after CD19 CAR-T cell therapy. Pharmacological inhibition of autophagy and knockout of RB1CC1 could dramatically sensitize tumor cells to CD19 CAR-T cell-mediated killing in mouse models of both B-cell leukemia and lymphoma. Moreover, our study revealed that cancer-intrinsic autophagy mediates evasion of CAR-T cells via the TNF-α-TNFR1 axis-mediated apoptosis and STAT1/IRF1-induced chemokine signaling activation.

Conclusions: These findings confirm that autophagy signaling in B-cell malignancies is essential for the effective cytotoxic function of CAR-T cells and thereby pave the way for the development of autophagy-targeting strategies to improve the clinical efficacy of CAR-T cell immunotherapy.

KEYWORDS
CAR-T resistance, Autophagy, Immune evasion, Apoptosis, Chemotaxis

1 | BACKGROUND

The successes with chimeric antigen receptor T (CAR-T) cell therapy for hematologic malignancies have revolutionized anticancer immunotherapy [1]. To date, the U.S. Food and Drug Administration (FDA) has approved six CAR-T cell products, including anti-CD19 CARs for the treatment of relapsed/refractory (R/R) B-cell acute lymphoblastic leukemia (B-ALL), diffuse large B-cell lymphoma (DLBCL) and mantle cell lymphoma (MCL), and the anti- B-cell maturation antigen (BCMA) CARs for multiple myeloma (MM). Nevertheless, as more patients are being treated and longer follow-up data are becoming available, it has been realized that approximately 10%-20% of $CD19^+$ R/R B-ALL patients who received the infusion of CD19 CAR-T cells failed to achieve complete remission (CR) within 3 months, and approximately 30%-50% of patients who achieved remission with CAR-T therapy suffered from relapse, most commonly within 1 year after treatment [2, 3]. Therefore, therapeutic failure due to cancer resistance and relapse constitutes a major obstacle to the broad application of CAR-T cell therapy.

Understanding the mechanism of resistance to CAR-T cells would facilitate the development of novel therapeutic strategies to overcome treatment failure and further refine CAR-T cell-based immunotherapy. Cancer resistance to

CAR-T cell therapy typically has two typical forms: the primary resistance (lack of responsiveness to CAR-T cell infusion) and the acquired resistance (disease relapse after initial remission) [4]. The common mechanism associated with relapse after CAR-T cell therapy is target antigen loss, making the molecule unrecognizable to CAR-T cells, with some of them being antigen-negative and others antigen-low [5–8]. In addition, the cell-intrinsic programs of CAR-T cells also play an important role in the functional impairment of CAR-T cells and may lead to therapeutic failure [5, 9-12]. Although tremendous efforts have been made to investigate factors that dictate the short- and long-term efficacy of CAR-T cell therapy [4-6, 13], the cancer-intrinsic mechanisms underlying resistance to CAR-T cells remain yet to be fully understood.

The whole-genome knockout screening constitutes a powerful tool for genetic studies and can be used to identify novel genes that contribute to certain biological phenotypes [14–16]. Lawson et al.[17] performed genome-wide clustered regularly interspaced short palindromic repeat (CRISPR) screens across a panel of genetically-diverse mouse cancer cell lines and identified a phenotypically robust core set of genes and pathways that enable tumor cells to evade killing mediated by cytotoxic T lymphocytes (CTLs). Thus, the high-throughput and efficient screening based on CRISPR/Cas9 genome-editing is an attractive technique for discovering key genes that sensitize tumors to or protect them from immunotherapy [17–21]. In another study, liquid and solid tumors were found to differ in their interactions with CAR-T cells [22]. In solid tumors, the interferon-γ receptor (IFNγR) signaling was required for sufficient adhesion of CAR-T cells to mediate productive cytotoxicity [22]. Furthermore, previous studies have documented through genome-wide loss-of-function screens that impaired death receptor signaling in B-ALL led to the rapid exacerbation of disease despite the CD19 CAR-T cell therapy [23, 24]. Since the mechanisms underlying cancer cell sensitivity to CAR-T cell-mediated cytotoxicity are fairly complicated and diverse, further knowledge of cancer-intrinsic evasion is urgently warranted.

This study aims to explore the molecular determinants of cancer cell sensitivity to CAR-T cell-mediated killing and to provide a better understanding of the underlying mechanisms and potential modulation to improve clinical efficacy. Here, we performed an unbiased CRISPR/Cas9 loss-of-function screen in the Nalm6 cell line under selection pressure from CD19 CAR-T cells. On the basis of the preliminary screening data, we speculatively proposed that autophagy might promote cancer resistance to CAR-mediated cytotoxicity in B-cell malignancies, and this hypothesis was further substantiated in cell lines, mouse models, and clinical samples. Collectively, our work revealed that autophagy was mechanistically implicated in cancer-intrinsic resistance and thereby paved the way for the development of mechanism-based strategies to improve the clinical efficacy of CAR-T cell immunotherapy.

2 | MATERIALS AND METHODS

2.1 | Cell lines and cell culture

The human cell lines Nalm6, Raji, Sup-B15, CA46, Romas and HEK 293T cell lines were purchased from American Type Culture Collection (ATCC, Manassas, VA, USA). The mouse cell line A20 was purchased from Zhong Qiao Xin Zhou Biotechnology Co., Ltd (Shanghai, China). CD19-K562 cells were kindly provided by Wuhan Si'an Medical Technology Co., Ltd (Wuhan, China). The identities of these cell lines were verified by short tandem repeat DNA sequencing analysis. Cell lines were cultured in 1640 Roswell Park Memorial Institute (RPMI; Gibco, NY, Grand Island, USA) or Dulbecco's Modified Eagle's Medium (DMEM, Gibco, NY, Grand Island, USA) supplemented with 10% fetal bovine serum (FBS; Gibco, NY, Grand Island, USA), 1% penicillin and streptomycin (Sigma-Aldrich, St Louis, MO, USA) at 37°C in 5% ambient carbon dioxide (CO_2), and tested regularly for mycoplasma contamination.

2.2 | CAR-T cell manufacturing

The pGEM-T plasmid, psPAX2 packaging plasmid and PMD2.G (Addgene, Watertown, USA) envelope plasmid were transfected into HEK 293T cells. Lentiviral supernatants were harvested 48 hours later and stored at -80°C. Peripheral blood mononuclear cells (PBMCs) were obtained from healthy donors by density gradient centrifugation, and $CD3^+$ T cells were isolated by using positive magnetic selection (human $CD3^+$ T Cell MicroBeads, Miltenyi Biotec, Bergisch Gladbach, Germany). Primary $CD3^+$ T cells were cultured in the X-VIVO 15 medium (Lonza, Basel, Switzerland) containing 10% FBS (Gibco, NY, Grand Island, USA) and 200 U/mL recombinant human IL-2 (200 IU/mL, PeproTech, Cranbury, NJ, USA). The anti-CD3 monoclonal antibody (OKT3, 2 μg/mL, Biolegend, San Diego, CA, USA) and anti-CD28 monoclonal antibody (CD28.2, 2 μg/mL, Biolegend, San Diego, CA, USA) were pre-coated overnight at 4°C to activate $CD3^+$ T cells. After 48 hours, the virus supernatant was added to the activated $CD3^+$ T cells. CAR-T cells were then replaced with fresh medium after 48 hours, and the cells were maintained in the X-VIVO 15 medium (Lonza, Basel, Switzerland)

containing recombinant human IL-2. The expression of CAR was measured to evaluate transfection efficacy on the third day. The detection of CD19 CAR-T cells was conducted by flow cytometry using Rabbit Anti-Mouse FMC63 sCFv MonoclonalAntibody PE detection reagent (200106, BIOSWAN, Shanghai, China) and PE Streptavidin (B367818, Biolegend, San Diego, CA, USA).

2.3 | CRISPR/Cas9 knockout library and genome-wide screening

CRISPR/Cas9 loss-of-function screening was performed using one human genome-wide single-guide RNA (sgRNA) library developed by Zhang's laboratory (www.genome engineering.org). The human GeCKOv2.0 sgRNA lentiviral knockout library was purchased from Shanghai Genechem Company (Shanghai, China). A total of 2 $\times 10^8$ Nalm6 cells were transduced at a multiplicity of infection (MOI) of 0.3 to ensure a single viral entry and selected with puromycin for stable integration for 7 days. Viral supernatants were used directly for spinoculation in a 1:1 mixture with growth medium in the presence of 5 ug/mL polybrene (Thermo Fisher Scientific, Waltham, MA USA). Centrifugation was carried out at 2,500 revolutions per minute (rpm) for 2 hours at 30°C. Then, 5×10^6 Nalm6 cells were collected for initial quality assessment. After puromycin selection, transduced Nalm6 cells were further cultured to 1.2 $\times 10^8$ and were then co-cultured with CD19 CAR-T cells at an effector:target (E:T) ratio of 1:10 or with vehicle alone. Approximately 48 hours after the addition of CD19 CAR-T cells, the remaining viable Nalm6 cells were separated and harvested using magnetic-activated absorption cell sorting (MACS). The human CD3 MicroBeads and Dead Cell Removal Magnetic Bead Kit was purchased from Miltenyi Biotec (Bergisch Gladbach, Germany).

2.4 | Genomic DNA sequencing and data analyses

Genomic DNA extraction (QIAGEN, Dusseldorf, Germany) and polymerase chain reaction (PCR) amplification were conducted according to the Zhang laboratory protocols [14, 15]. For each sample, we performed at least 100 separate 50 μL reactions, with 2 μg of genomic DNA in each reaction. We used NEB Next High-Fidelity DNA Polymerase (New England BioLabs, Ipswich, Massachusetts, USA) and the default mixture protocol with the following thermal cycling parameters for PCR (98°C for 3 minutes; 24 cycles of 98°C for 10 seconds, 63°C for 10 seconds, and 72°C for 25 seconds; 72°C for 2 minutes). After the reaction was completed, we pooled the amplification products and purified them by using the QIAquick Gel Extraction Kit (QIAGEN, Dusseldorf, Germany) according to the manufacturer's instructions. The purified, pooled library was quantified using the Qubit dsDNA HS Assay Kit (Thermo Fisher Scientific, Waltham, MA USA) according to the manufacturer's instructions and was then sequenced on the Illumina MiSeq platform (San Diego, California, USA) with a 5% PhiX added to the sequencing lane. For analysis of the pooled CRISPR screening data, we first normalized the data by multiplying the read count for each sample by a scaling factor so that all the samples had the same total read count. We analyzed the next-generation sequencing (NGS) results in "fastq_file" for the guide representation by counting the number of reads that contained a perfectly matched guide in the "library_sequences" file and wrote the results to the "output_file" using a Python script provided by the Zhang' laboratory [14]. For group comparisons, the normalized read count tables were used as inputs to Model-based Analysis of Genome-Wide CRISPR-Cas9 Knockout (MAGeCK; version 0.5.8, https://sourceforge.net/projects/mageck/), with one group designated as the treatment group and the other as the control [25].

2.5 | Lentiviral packaging and cell transfection

For validation experiments, oligonucleotides targeting different genes were annealed, sub-cloned and inserted into the lenti-CRISPRv2 vector (Addgene, Watertown, USA). The sgRNA vectors were then transfected into HEK 293T cells, together with the pMD2.G and psPAX2 vectors, using Lipofectamine-3000 (Invitrogen, Thermo Fisher Scientific, Waltham, MA USA) following the protocols recommended by the manufacturer. Similarly, the short hairpin RNA (shRNA) vectors were transfected into HEK 293T cells together with pMD2.G and psPAX2 vectors, using Lipofectamine-3000 by following the protocols recommended by the manufacturer. The medium were replaced after 24 hours, and the viral supernatant was collected 72 hours post-transfection by high-speed ultracentrifugation at 25,000 rpm and 4°C for 2 hours. Viruses were concentrated, and the titers were determined by using TransLv^{TM} Lentivirus qPCR Titration Kit (ABM, Beijing, China). For viral transduction, Nalm6 and Raji cells were seeded into 6-well plates supplemented with 2 μg/mL polybrene (Invitrogen, Thermo Fisher Scientific, Waltham, MA USA) and transduced by spinoculation [26]. Centrifugation was carried out at 2,500 rpm for 2 hours at 30°C. The sgRNA- or shRNA-transduced cells were selected with an appropriate concentration of puromycin for 5-7 days to confirm stable integration. The sgRNA sequences used for

CRISPR/Cas9-mediated gene knockout are presented in Supplementary Table S1. The shRNA sequences used for gene knockdown are presented in Supplementary Table S2.

2.6 | in vitro cytotoxicity and apoptosis assay

To determine the effect of targeting autophagy on the cytotoxicity of CD19 CAR-T cells, Nalm6, Raji, SUP-B15 and K562-CD19 cells were used for cytotoxicity assays. Malignant B cells were obtained from two patients with B-ALL by human CD19 MicroBeads (130-050-301, Miltenyi Biotec, Bergisch Gladbach, Germany). Cancer cells were pretreated with autophinib (Selleck, S8596, 2 μmol/L, Shanghai, China), SAR405 (Selleck, S7682, 2 μmol/L, Shanghai, China), C hloroquine (Selleck, S6999, 1 μmol/L, Shanghai, China), Hydroxychloroquine Sulfate (Selleck, S6999, 1 μmol/L, Shanghai, China) and rapamycin (Selleck, AY-22989, 0.1 nmol/L, Shanghai, China) for 72 hours before the co-culture with CD19 CAR-T cells. Infliximab (Selleck, A2019, 1 ug/mL, Shanghai, China) was used to block TNF-α. Cancer cells were prestained with 1 μmol/L CFSE (5, 6- carboxyfluorescein diacetate, succinimidyl ester, BD Biosciences, San Jose, CA, USA). CD19 CAR-T cells and target tumor cells were co-cultured at different E:T ratios (0:1, 1:4, 1:2 and 1:1) at 37 °C for 24 hours. Cancer cell killing was analyzed by using propidium iodide (PI, Biolegend, 0.2 μg/mL, San Diego, CA, USA) staining and flow cytometry. For observation of apoptosis of tumor cells, CFSE-labeled tumor cells were co-cultured with or without CAR-T cells at an E:T ratio of 1:10 for 24 hours, and then the apoptosis assay was conducted with the Annexin V/7-aminoactinomycin D (7-AAD) using the protocol provided with the apoptosis detection kit (A213-01, Nanjing Vazyme Biotech Co, Ltd, Nanjing, China).

2.7 | Clinical tissue specimens and immunohistochemistry (IHC)

Tumor tissue samples before CD19 CAR-T cell infusion were obtained from patients with B-cell lymphoma in a clinical trial (NCT04008251, "Treatment of Relapsed or Refractory B-cell Malignancies by Humanized CD19 Chimeric Antigen Receptor (CAR)-Modified T Cells"). The inclusion and exclusion criteria for NCT04008251 are provided in Supplementary Materials and Methods 1. The study was agreed with informed consent obtained from all subjects and approved by the Ethics Committee of the Union Hospital affiliated with Huazhong University of Science and Technology, Wuhan, China (REC ref no. [2019]008). We retrospectively collected the relevant data, including tumor type, sex, age, response or not, duration of response, survival, etc. Pathological biopsy was performed mainly in swollen lymph nodes or localized tumor masses in patients with B-cell lymphoma. The tumor tissue samples were further stained with ATG3 (Abcam, ab108282, 1:100, Cambridge, UK), RB1CC1 (Proteintech, 17250-1-AP, 1:100, Rosemont, USA), BECN1 (Proteintech, 11306-1-AP, 1:200, Rosemont, USA), phosphorylated signal transducer and activator of transcription 1 (pSTAT1, Cell Signaling, #9167, 1:200, Boston, IL, USA) antibodies by IHC. The IHC scores were calculated according to the staining intensity (0/1/2/3) and positive staining rate (grouped into quartiles and assigned scores of 0 to 4). The staining intensity and positive staining rate scores were multiplied to obtain the final IHC score. Scores ranging from 0 to 4 were considered to indicate low expression, and scores that exceeded 4 were considered to indicate high expression.

2.8 | Immunofluorescence staining

Cells were spun onto poly-l-lysine (Sigma Aldrich, St Louis, MO, USA)-coated coverslips, washed with phosphate-buffered saline (PBS) and fixed with 4% paraformaldehyde overnight (12 to 16 hours). Cells were incubated with primary antibodies at 4°C overnight with the fluorescent secondary antibodies for one hour. The CD3 (Proteintech, 60181-1-Ig, 1:200, Rosemont, USA), LC3B (Cell Signaling, #43566, 1:6,000, Boston, IL, USA), PD-1 (Cell Signaling, #86163, 1:200, Boston, IL, USA), CD69 (Proteintech, 10803-1-AP, 1:100, Rosemont, USA), dsDNA (Santa Cruz Biotechnology, sc-58749, 1:100, Dallas, USA) antibodies were used for immunofluorescence staining. Nuclei were stained with 4',6-diamidino-2-phenylindole (DAPI, Cell Signaling, #4083, Boston, IL, USA) for 10 minutes, and the cells were then analyzed by confocal microscopy (Andor, Dragonfly, 633 objective lens, Oxford, England). For colocalization analysis, fluorescence intensity profiles were generated for each channel using NIS Elements software (Nikon Precision Shanghai Co., Ltd., Shanghai, China). An area of overlap between the peaks in two channels was considered as a double-positive area.

2.9 | Cytokine secretion assay

LEGENDplex^{TM} assays (BioLegend, San Diego, CA, USA) were used to assess the secretion of cytokines. These assays are bead-based immunoassays, which are, in terms of principles, similar to sandwich immunoassays. For the analysis of cell supernatants, cells were deprived of serum, and interleukin 6 (IL-6), IL-10, TNF-α, IFN-γ and IL-2 were quantified using the Human Th1 Panel (5-Plex)

(BioLegend, No. 741035, San Diego, CA, USA) following the manufacturer's instructions.

2.10 | RNA sequencing and bioinformatic analysis

After the Nalm6 cells were treated with vehicle and autophinib (Selleck, S8596, 2 μmol/L) for 72 hours, the sgControl and RB1CC1 knockout (RB1CC1^{KO}) Nalm6 cells were collected for RNA sequencing. RNA extraction, library construction and sequencing were performed by the Beijing Novogene Company (Beijing, China). For bulk RNA sequencing analysis of bone marrow samples from patients treated with CD19 CAR-T cell therapy, we analyzed the data set from GSE153670. The differentially-expressed genes were defined as genes with a P value <0.05 and a $\log_2$ fold change ($\log_2$FC) of >1. The EdgeR package was used for data normalization and gene variance analysis. Kyoto Encyclopedia of Genes and Genomes (KEGG) enrichment analysis and gene set enrichment analysis (GSEA) [27] were performed. Receiver operating characteristic (ROC) analysis was conducted to identify a threshold gene set score with high positive and negative predictive values of clinical outcomes in the sample set. Visualization was performed using the R package ggplot2.

2.11 | Tumor xenograft models

All in vivo animal experiments were approved by the Ethics Committee of Tongji Medical College, Huazhong University of Science and Technology (IACUC No. 2727), Wuhan, China. Immunocompetent BALB-c (female, 5 weeks old) and immunodeficient M-NSG (male, 5 weeks old) mice were purchased from Vitalriver (Beijing, China) and housed under pathogen-free conditions for one week before use in experiments. Nalm-6 and Raji cells were transduced with lentiviral vector encoding green fluorescent protein-luciferase and then purified by fluorescence-activated cell sorting. All mice were randomly allocated into groups before receiving the treatment. To establish the A20 xenograft mouse model, 5×10^6 A20 cells diluted in 100 μL of PBS were injected subcutaneously into the right flank of BALB-c mice. Autophinib (20 mg/kg, Selleck, Shanghai, China) was intraperitoneally injected into the mice. SAR405 (10 mg/kg, Selleck, Shanghai, China) was given to the mice by oral gavage. To establish the intravenous xenograft mouse model, M-NSG mice were intravenously injected with 10^6 luc$^+$ (luciferase positive) Nalm6 or RB1CC1^{KO} luc$^+$ Nalm6 cells diluted in 100 μL of PBS. After 9 days of leukemia growth, 10^6 CD19 CAR-T cells in 100 μL of PBS were injected into mice via the tail vein. To establish the subcutaneous xenograft mouse model, 5×10^6 luc$^+$ Raji cells or RB1CC1^{KO} luc$^+$ Raji cells diluted in 100 μL of PBS were injected subcutaneously into the right flanks of M-NSG mice. After 7 days of subcutaneous tumor growth, 5×10^6 CD19 CAR-T cells in 100 μL PBS were injected into the mice via the tail vein.

Tumor burdens were monitored and quantified by bioluminescence imaging (BLI) on the Lago X Imaging System (Spectral Instruments Imaging, Arizona, USA). BLI signals are presented as the average radiance and acquired by Living Image software (Amiview, Arizona, USA). The subcutaneous tumors were measured using a caliper every three days, and tumor volumes were estimated as follows: tumor volume (mm^3) = $(\text{width})^2 \times \text{length} \times 0.5$. All subcutaneous xenografts were excised and weighed after all mice were euthanized. The excised subcutaneous tumor tissues were subsequently used for immunophenotyping by immunohistochemistry and flow cytometry. Tumors were fixed with 4% paraformaldehyde for 48 hours and then embedded in paraffin. After formalin fixation, paraffin-embedded tumor sections (5 μm thick) from different tumors were stained with the corresponding antibodies. The CD3 (Proteintech, 60181-1-Ig, 1:2,000, Rosemont, USA), CD4 (Proteintech, 67786-1-Ig, 1:400, Rosemont, USA), CD8 (Proteintech, 66868-1-Ig, 1:5,000, Rosemont, USA), and cleaved caspase-9 (Abcam, ab32068, 1:50, Oxford, England) antibodies were used for immunohistochemistry staining.

2.12 | Multiparametric flow cytometric analysis

To assess the function of CAR-T cells after co-cultured with tumor cells, cells were harvested after co-culture. For surface staining, cells were washed twice in PBS containing 1% FBS, and then were stained with fluorochrome-conjugated anti-human monoantibodies (mAbs). Samples were incubated with antibodies for 30 minutes at 4°C, and then washed with staining buffer. Intracellular staining for TNF-α, granzyme B, perforin, and CD107a was performed after cell fixation and permeabilization (eBioscience, Thermo Fisher Scientific, Waltham, MA USA), and then intracellular proteins were labeled with the corresponding mAbs conjugated with fluorescent molecules according to the manufacturer's instructions. Tumors were harvested and mechanically dissociated into fragments, and the fragments were then enzymatically digested using the Type IV collagenase (Gibco, NY, Grand Island, USA) and deoxyribonucleases I (Thermo Fisher Scientific, Waltham, MA USA) for 2 hours at 37°C. Single-cell suspensions were prepared, and red blood cells were removed by lysis buffer (Solarbio, Beijing, China). Cells were then counted on a Countess Automated Cell Counter

(Logos Biosystems, Luna, Los Angeles, Southern California, USA) and washed twice in PBS containing 1% FBS (staining buffer, BD Biosciences, San Jose, CA, USA). The samples were first stained for surface markers for lymphoid and myeloid immune populations and then subjected to intracellular staining. Before surface staining, the samples were blocked for 30 minutes on ice with Fc Block (BioLegend, San Diego, CA, USA) and were then stained with fluorochrome-conjugated anti-mouse antibodies. Samples were incubated with antibodies for 30 minutes at 4°C and were then washed with staining buffer. Intracellular staining for CD206 was performed after cell fixation and permeabilization (eBioscience, Thermo Fisher Scientific, Waltham, MA USA), and then intracellular proteins were then labeled according to the manufacturer's instructions. The reagent in the LIVE/DEAD Fixable Viability Stain Kit 780 (BD Pharmingen, FranklinLakes, New Jersey, USA) was used as a viability dye. The following antibodies were obtained from BioLegend (San Diego, CA, USA): FITC anti-mouse CD45, APC anti-mouse CD3, PerCP anti-mouse CD4, Brilliant Violet 605™ anti-mouse CD8a, PE/Cyanine7 anti-mouse NK-1.1, PE anti-mouse CD94, PE/Dazzle™ 594 anti-mouse CD366 (Tim-3), Brilliant Violet 510™ anti-mouse Ly-6C, PE/Cyanine7 anti-mouse Ly-6G, APC anti-mouse F4/80, Brilliant Violet 605™ anti-mouse CD206 (MMR), PerCP anti-mouse CD11c, PE anti-mouse/human CD11b, Brilliant Violet 421™ anti-mouse CD194 (CCR4), PE/Dazzle™ 594 anti-mouse CD196 (CCR6), PE/Cyanine7 anti-mouse CD127 (IL-7Rα), Alexa Fluor® 700 anti-mouse CD25, PE anti-mouse CD185 (CXCR5), Brilliant Violet 510™ anti-mouse CD183 (CXCR3), Brilliant Violet 421™ anti-mouse CD279 (PD-1), Brilliant Violet 510™ anti-mouse CD69 and Brilliant Violet 421™ anti-mouse CD16/32. Flow cytometry was performed with the BD LSRFortessa X-20 and Sony ID7000 spectral cell analyzer, and data were analyzed with FlowJo V10 software (Tree Star, Oregon, USA).

2.13 | SYBR Green real-time quantitative PCR (RT-qPCR)

Total RNA was extracted using TRIzol reagent (Invitrogen, Thermo Fisher Scientific, Waltham, MA USA) and Ultrapure RNA Kit (CWBIO, Jiangsu, China) and was further detected for RNA integrity and absence of DNA contamination. The total RNA was reverse transcribed into complementary DNA using a First Strand cDNA Synthesis Kit (Nanjing Vazyme Biotech Co, Ltd, Nanjing, China). An SYBR Green Master Mix Kit (Nanjing Vazyme Biotech Co, Ltd, Nanjing, China) was used to carry out RT-qPCR experiments according to the manufacturer's instructions. RT-qPCR experiments were conducted following the Minimum Information for Publication of Quantitative Real-Time PCR Experiments (MIQE) guidelines [28]. Two reference genes (GAPDH and β-actin) were used for data normalization. The primer was designed specifically for the exon-junction spanning part. The amplification efficiency of primers used in RT-qPCR should be between 90% and 110%, and the value of R^2 should be greater than or equal to 0.98. The primer sequences used for RT-qPCR were presented in Supplementary Table S3. RT-qPCR experiments were performed on a 7500 Fast System (Thermo Fisher Scientific, Waltham, MA USA).

2.14 | Western blotting

For Western blot analysis, cells were harvested and lysed with modified radio immunoprecipitation assay (RIPA, Beyotime, Shanghai, China) lysis buffer supplemented with protease inhibitor cocktail (Sigma-Aldrich, St. Louis, Missouri, USA) and phosphatase inhibitor cocktail (Thermo Fisher Scientific, Waltham, USA). Protein lysates were separated by sodium dodecyl sulfate–polyacrylamide gel electrophoresis (SDS–PAGE, Genscript, Nanjing, Jiangsu, China) and transferred onto polyvinylidene fluoride (PVDF) membranes (Genscript, Nanjing, Jiangsu, China). The membranes were next incubated with specific primary antibodies, and immunoreactions were detected by enhanced chemiluminescence. ImageJ (National Institutes of Health, Bethesda, Maryland, USA) was applied to quantify the expression of the proteins of interest. The following antibodies were used for Western blotting: ATG3 (Abcam, ab108282, 1:500, Oxford, England), RB1CC1 (Proteintech, 17250-1-AP, 1:2,000, Rosemont, USA), BECN1 (Proteintech, 11306-1-AP, 1:1,000, Rosemont, USA), p62 (Cell Signaling, #5114, 1:1,000, Boston, IL, USA), LC3B (Cell Signaling, #43566, 1:1,000, Boston, IL, USA), TNFR1 (Proteintech, 21574-1-AP, 1:1,000, Rosemont, USA), pSTAT1 (Cell Signaling, #9167, 1:1,000, Boston, IL, USA), STAT1 (Cell Signaling, #14994, 1:1,000, Boston, IL, USA), IRF1 (Proteintech, 11335-1-AP, 1:1,000, Rosemont, USA), IRF4 (Proteintech, 11247-1-AP, 1:1,000, Rosemont, USA), IRF7 (Abcam, ab238137, 1:1,000, Oxford, England), Caspase-8 (Proteintech, 66093-1-Ig, 1:1,000, Rosemont, USA), Caspase-9 (Proteintech, 66169-1-Ig, 1:1,000, Rosemont, USA), cleaved Caspase-8 (Cell Signaling, # 9748, 1:1,000, Boston, IL, USA), cleaved Caspase-9 (Abcam, ab2324, 1:1,000, Oxford, England) and GAPDH (Proteintech, 60004-1-Ig, 1:8,000, Rosemont, USA).

2.15 | Chemotaxis assay

The human CD19 CAR-T cells (2×10^6 cells /ml, 200 μL per well) in the X-VIVO 15 medium were added to the top

chambers of the 24-well Transwell plates (80 μm pores; Corning, Lowell, MA, USA). The Nalm6 (10^6/mL) and Raji (10^6/mL) cells were cultured in RPMI 1640 medium (with 10% FBS) with autophinib (2 μmol/L, Selleck, Shanghai, China) and rapamycin (0.1 nmol/L, Selleck, Shanghai, China) for 72 hours. The Nalm6 (10^6/mL) and Raji (10^6/mL) cells with sgControl and RB1CC1 knockout were cultured in RPMI 1640 medium (with 10% FBS) for 72 hours. The culture supernatants were collected and added to the bottom chambers (600 μL per chamber). After 4 hours, the migrated CD19 CAR-T cells were counted, and migration was quantified by flow cytometry.

2.16 | Enzyme-linked immunosorbent assay (ELISA)

Cancer cell supernatants were obtained after in vitro culture under serum deprivation conditions. CXCL9, CXCL10 and CXCL11 were quantified using the human CXCL9/MIG Quantikine ELISA Kit (DCX900, R&D Systems, Minnesota, USA), human CXCL10/IP-10 Quantikine ELISA Kit (DIP100, R&D Systems, Minnesota, USA) and human CXCL11/I-TAC Quantikine ELISA Kit (DCX110, R&D Systems, Minnesota, USA), respectively, following the manufacturer's instructions.

2.17 | Chromatin immunoprecipitation (ChIP)-qPCR

The chromatin extraction kit (Abcam, ab117152, Oxford, England) and ChIP Kit Magnetic-One Step (Abcam, ab156907, Oxford, England) were used to carry out the ChIP for the selective enrichment of a chromatin fraction containing specific DNA sequences from isolated chromatin to investigate the interaction between proteins and DNA. The primer sequences used for ChIP-qPCR are listed in Supplementary Table S4.

2.18 | Statistical analysis

All data were statistically analyzed and visualized using GraphPad Prism software (version 8.0, San Diego, California, USA). All experiments were repeated independently at least twice. All comparisons between two groups were performed using either a two-tailed unpaired Student's t test or the Mann–Whitney U test, depending on the normality of the distribution. Comparisons between more than two groups were performed by one-way analysis of variance (ANOVA), two-way ANOVA and Tukey's multiple comparisons test. All results are represented as means ± standard deviations (SDs) or medians with ranges. Survival data were analyzed using the log-rank (Mantel-Cox) test. A P value of less than 0.05 was considered to indicate a statistically significant difference ($^*P < 0.05$; $^{**}P < 0.01$; $^{***}P < 0.001$; $^{****}P < 0.0,001$; ns: not significant).

3 | RESULTS

3.1 | Genome-wide CRISPR screening identifies autophagy-mediated resistance to CAR-T cells

To identify key genes that modulate the susceptibility of B-cell malignancies to CD19 CAR-T cell-mediated killing, we performed a CRISPR screening based on the genome-wide knockout library in Nalm6 cells (Figure 1A). The specific structure of anti-CD19 CAR used in this study is presented in Supplementary Figure S1A-B Nalm6 cells were transfected with the CRISPR/Cas9 lentivirus sgRNA library (Human GeCKO v2.0) and then subjected to puromycin selection. Nalm6 cells with CRISPR-mediated knockouts were co-cultured with CD19 CAR-T cells at a low E:T ratio. The MAGeCK results of CRISPR/Cas9 library screening are provided in Supplementary Table S5. CRISPR screening and sgRNA sequencing (Figure 1B) demonstrated significant depletion of guides targeting genes in the autophagy pathway (*ATG3*, *BECN1*, *RB1CC1*), as well as the enrichment of guides targeting proapoptotic and tumor necrosis factor (TNF) signaling-related molecules. KEGG functional pathway enrichment analysis of the most highly depleted and enriched sgRNAs identified enrichment in pathways involved in tumor immune modulation, such as autophagy-animal, apoptosis, TNF signaling and cytokine-cytokine receptor interaction (Figure 1C). We next investigated the clinical relevance of autophagy in the therapeutic response to and relapse after CAR-T cell therapy in patients with R/R B-cell malignancies. Based on the preliminary screening results, we examined the expression of three autophagy-related proteins, ATG3, BECN1, and RB1CC1 [29]. The IHC staining was used to quantify the ATG3, BECN1 and RB1CC1 protein levels in available tumor tissue samples that were obtained before CD19 CAR-T-cell therapy and collected from responders who achieved a complete response and non-responders. The protein levels of ATG3, BECN1 and RB1CC1 were significantly higher in the non-responder group than in the responder group (Figure 1D-G). The ROC suggested a strong correlation (AUC = 0.906, $P = 0.027$) between the high expression of the three proteins in tumor samples and poor responsiveness to CAR-T cell infusion (Figure 1H). Furthermore, the Kaplan-Meier survival analysis revealed

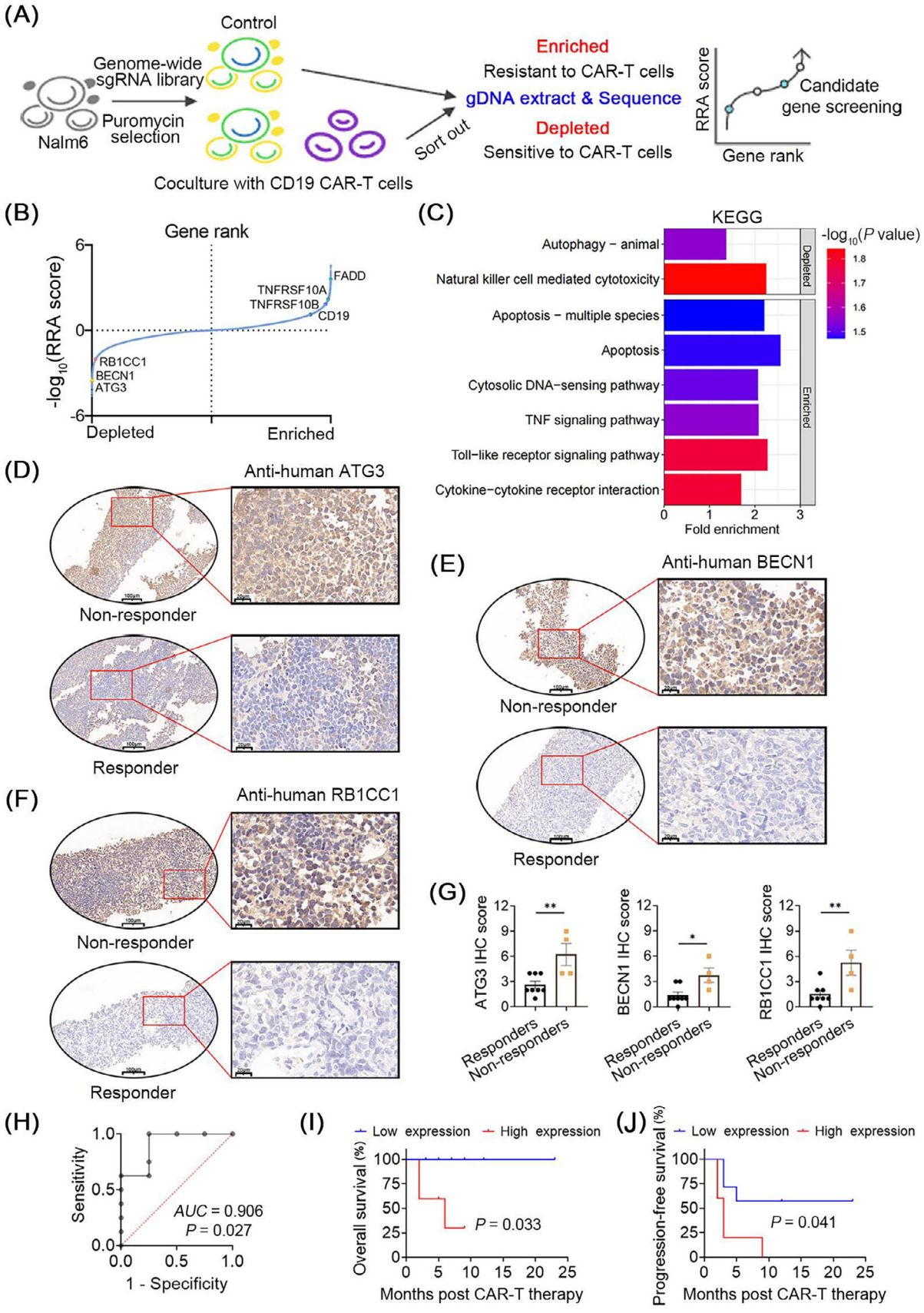

FIGURE 1 Genome-wide CRISPR screening identifies essential genes mediating resistance to CAR-T cells. (A) Schematic of pooled CRISPR knockout screening for Nalm6 cell sensitivity to the killing mediated by CD19 CAR-T cells. (B) Ranking diagram showing genes that either promote (enriched sgRNAs) or suppress (depleted sgRNAs) tumor cell killing. (C) KEGG pathway enrichment analysis of most

that high protein levels of these three autophagy-related proteins were associated with worse progression-free survival and overall survival (Figure 1I). Since mTOR activation could inhibit autophagic activity, we also detected the protein levels of mTOR in tumor samples. The protein level of mTOR was significantly lower in the non-responders than in responders (Supplementary Figure S2A), and the expression of the three autophagy markers was also negatively correlated with the expression of mTOR (Supplementary Figure S2B). Additionally, the bulk RNA sequencing analysis of bone marrow samples of B-cell leukemia patients from the dataset GSE153670 [23] further validated the association between the expression of autophagy- and apoptosis-related genes in leukemic cells and clinical outcomes after CD19 CAR-T cell therapy. By conducting the KEGG pathway enrichment analysis of the differentially expressed genes, we found that the autophagy, apoptosis and TNF signaling pathways were involved in the development of resistance to CAR-T cells (Supplementary Figure S3A-B). Moreover, the ROCs indicated that these signaling pathways had strong discriminatory power for clinical responsiveness after CAR-T cell infusion (Supplementary Figure S3C) and might serve as predictive biomarkers during CAR-T cell therapy.

3.2 | Targeting autophagy sensitizes B-cell malignancies to CAR-T cell-mediated cytotoxicity in vitro

To further confirm these observations and elucidate the role of autophagy in cancer cell susceptibility to CAR-T cells, we used three kinds of autophagy-related chemical autophagy modulators: rapamycin (an autophagy inducer), SAR405 and autophinib (autophagy inhibitors). As a regulatory factor, P62 (also called SQSTM1) participates in the formation of autophagosomes and is degraded in the middle and late stages of autophagy [29, 30]. Generally, the conversion of LC3-I to LC3-II via conjugation to phosphatidylethanolamine initiates the formation and elongation of the autophagosome [29–31]. Thus, the degradation of P62 indicates an increase in autophagic activity, and the ratio of LC3-II/LC3-I is positively correlated with autophagic activity [29–31]. Indeed, autophagic activity in Nalm6 and Raji cells was affected by rapamycin, SAR405 and autophinib, as indicated by the levels of the autophagy cargo receptor p62 and autophagosome marker LC3B-II (Figure 2A). The data of LC3B IF staining also suggested that autophagic activity in Nalm6 and Raji cells was affected by rapamycin, SAR405 and autophinib (Figure 2B-C). When co-cultured with CAR-T cells in vitro at low E:T ratios for 24 hours, the pre-treatment of tumor cells with autophagy inhibitors (SAR405 and autophinib) before the co-culture significantly enhanced the killing effect of CD19 CAR-T cells, whereas the pre-treatment with the autophagy inducer (rapamycin) exerted diametrically opposed effects (Figure 2D, Supplementary Figure S4A-B). The pre-treatment of SAR405, autophinib and rapamycin had no effect on the expression of CD19 protein (Supplementary Figure S4C). To extend our observation, we performed cytotoxicity assays on two other tumor cell lines that showed high-level autophagic activity. The pre-treatment of autophinib or SAR405 in the other two lymphoma cell lines (CA46 and Romas) significantly increased the CD19 CAR-T-specific killing (Supplementary Figure S4D). Moreover, consistent findings were also observed in cytotoxicity analysis applied to malignant B cells obtained from two patients with B-ALL (Supplementary Figure S4E-F). We next attempted to validate our results through a genetic approach and examined the role of autophagy-related genes in cancer cell sensitivity to CAR-T cells. The knockout of ATG3, BECN1 and RB1CC1 using CRISPR/Cas9-based genome editing diminished the autophagic activity in Nalm6 and Raji cells (Figure 2E-H) but had no effect on the expression of CD19 protein (Figure 2I-J). As expected, consistent results were observed upon knockout of the three autophagy-related genes, further validating the protective role of autophagy (Figure 2K). The ectopically rescued expression of RB1CC1 attenuated the promotion of CAR-T cell-mediated cytotoxicity (Supplementary Figure

differentially-expressed genes identified in CRISPR screening. (D-F) Representative images of IHC staining for high and low protein expression of ATG3, BECN1 and RB1CC1 in R/R B-cell lymphoma before treatment with CD19 CAR-T cell therapy. The outlined areas in the left images are magnified on the right. Scale bars, 50μm. (G) IHC scores in tumor samples from responders ($n = 8$) and non-responders ($n = 4$). Values are shown as the mean ± SD. The unpaired Student's t test was used to analyze the differences between two groups. (H) The ROC showing the strong correlation between high expression of the three proteins in tumor samples and poor responsiveness to CAR-T cell infusion. (I-J) Kaplan–Meier plots of overall survival and progression-free survival between two groups B-cell lymphoma patients with low and high expression of ATG3, BECN1 and RB1CC1 as evaluated by IHC. Log-rank tests were used to analyze the significance between the two groups. *$P < 0.05$; **$P < 0.01$. Abbreviations: CAR-T chimeric antigen receptor T; CRISPR clustered regularly interspaced short palindromic repeat; KEGG Kyoto Encyclopedia of Genes and Genomes; ROC receiver operating curve; IHC immunohistochemistry; R/R relapsed/refractory; RRA robust rank aggregation; sgRNA single-guide RNA.

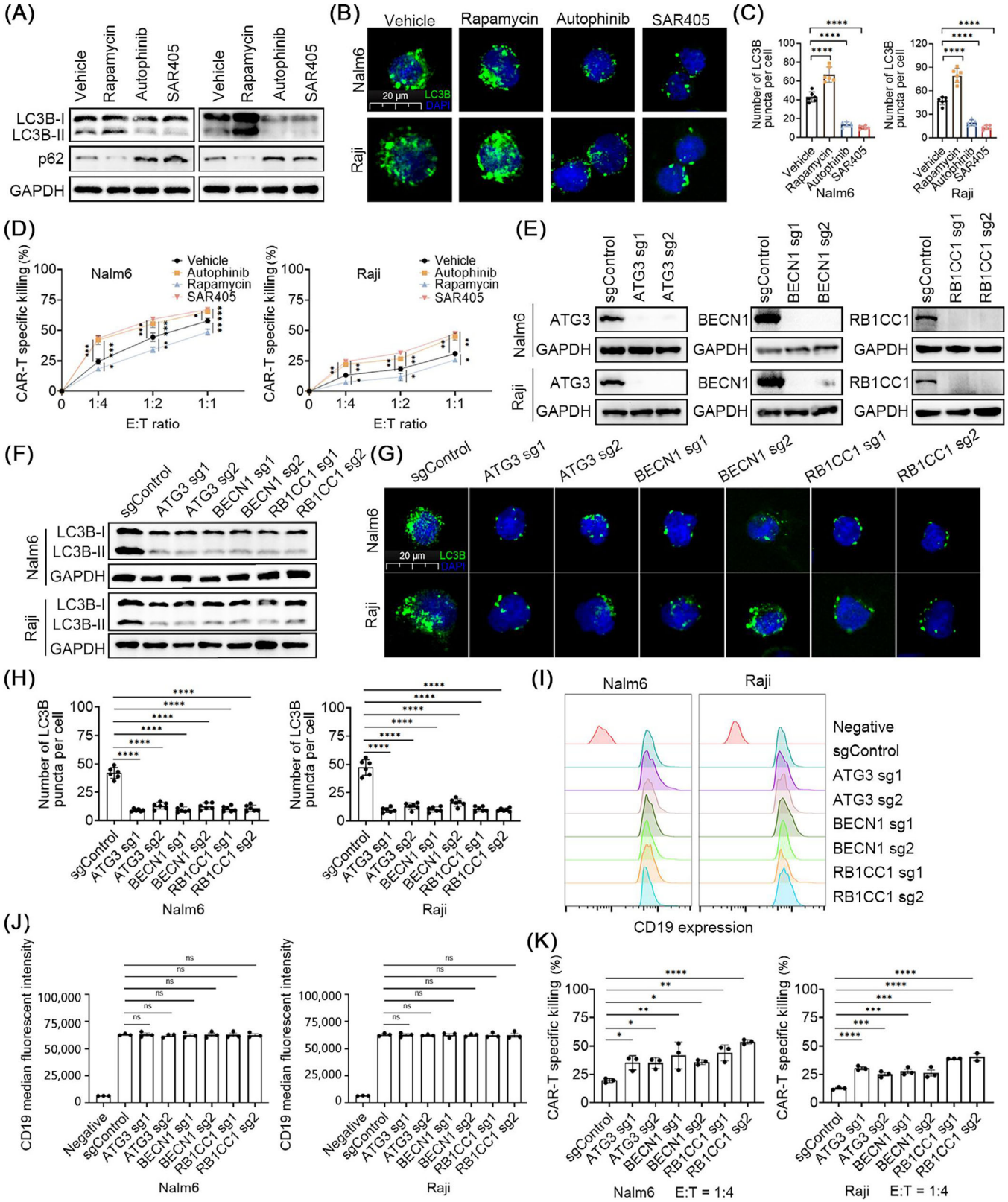

FIGURE 2 Autophagy protects B-cell malignancies from CAR-T cell-mediated cytotoxicity in vitro. (A) Western blotting showing the expression levels of p62 and LC3B proteins 72 hours after the addition of vehicle (as control), rapamycin, SAR405 and autophinib in Nalm6 and Raji cell lines. GAPDH was used as a loading control. (B-C) Representative images of LC3B immunofluorescent staining of Nalm6 and Raji cells treated with vehicle (as control), rapamycin, SAR405 and autophinib. Number of LC3B puncta per cell was compared between the three groups ($n = 6$). Values are shown as the mean ± SD. Differences among groups were calculated with one-way ANOVA tests. (D) Cytotoxic analysis of vehicle, rapamycin, SAR405 and autophinib pre-treated Nalm6 and Raji cell lines when co-cultured with CD19 CAR-T

S4G). Moreover, the pre-treatment of hydroxychloroquine and chloroquine could also promote CAR-T cell-mediated killing, indicating their therapeutic potential in the clinic (Supplementary Figure S4H). The findings suggest that genetic inhibition of autophagy increases sensitivity to CAR-T immunotherapy via a mechanism independent of the CD19 CAR target. We then assessed the functions of CAR-T cells after co-culturing with tumor cells, including the expression of activation markers, cytotoxic molecules and exhaustion markers. The pre-treatment of autophinib showed no impacts on the expression of CD28, CD57, CD69 and PD-1 in CAR-T cells after co-culture with Nalm6 and Raji cells (Supplementary Figure S5A-B). Interestingly, regarding cytotoxic molecules, inhibiting the autophagic activity in tumor cells enhanced the expression of granzyme B from CAR-T cells after co-culture in the E:T ratios of 1:4 and 1:1 (Supplementary Figure S5C-D). Therefore, we postulated that cancer-intrinsic autophagy may promote the resistance of B cell malignancies to CAR-mediated cytotoxicity in vitro, but the underlying mechanisms remain to be further explored.

3.3 | Targeting autophagy enhances the anti-tumor activity of CAR-T cells by promoting TNF-α-TNFR1 axis-mediated apoptosis

We conducted RNA sequencing on control and autophagy-targeted cells to identify the transcriptional networks. Further analysis showed significant changes in gene expression upon treatment with autophinib or knockout of RB1CC1 (Figure 3A-B, Supplementary Table S6 and Table S7). KEGG pathway enrichment analysis of significantly-upregulated genes indicated a prominent role of the apoptosis pathway in leukemia cells (Figure 3C), which was consistent with previous results [24, 32, 33]. We further found that pharmacological inhibition of autophagy induced caspase8 and caspase9 cleavage in tumor cells when they were co-cultured with CD19 CAR-T cells (Figure 3D), while pharmacological induction of autophagy showed the opposite results (Supplementary Figure S6A-B). The knockout of BECN1 and RB1CC1 also exhibited promotion in apoptosis (Figure 3E). Moreover, the results of Annexin V/7-AAD double staining (Supplementary Figure S7A) suggested that both pharmacological (Supplementary Figure S7B-E) and genetic (Supplementary Figure S7F-I) inhibition of autophagy resulted in a substantial increase in tumor cell apoptosis after co-culture with CD19 CAR-T cells. As autophagy has been proposed to inhibit apoptosis via multiple pathways [34], we therefore conducted a series of experiments to gain insights into the underlying mechanism. Although killing by cytotoxic T cells is thought to result primarily from granule exocytosis triggered by the release of perforin and granzyme from T cell granules, the roles of TNF and other death receptor ligands in this process have been previously proposed [35]. TNF can promote cell death via either apoptosis or necroptosis [35, 36]. Thus, we explored the role of TNF-α-induced apoptosis following autophagy targeting in cancer cell resistance to CAR-T cells, which was indicated based on the results of CRISPR screening and transcriptomic analysis. Notably, the TNF-α receptor TNFRSF1A (encoding TNFR1) was significantly up-regulated at both the transcriptional and translational levels after autophagy inhibition (Figure 3F). Further analysis of the ChIP-Atlas database suggested the presence of STAT1 binding peaks in the promoter region of TNFRSF1A (Supplementary Figure S8A). Moreover, the mRNA level of STAT1 was increased in Nalm6 and Raji cells treated with autophagy inhibitors (Supplementary Figure S8B-C). Western blotting analysis showed that the TNFR1 protein level was decreased when STAT1 was silenced (Supplementary Figure S8D-E). The ChIP-qPCR results further validated the binding of STAT1 to the promoter region of TNFRSF1A (Supplementary Figure S8F). TNFR1 induction was no longer observed in both autophagy inhibitor-treated Nalm6 or Raji cells when

cells at different E:T ratios (0:1, 1:4, 1:2, 1:1) at 37 °C for 24 hours ($n = 3$). Values are shown as the mean ± SD. Differences among groups were calculated with two-way ANOVA tests. (E) Western blotting showing the expression levels of three autophagy-related (ATG3, BECN1 and RB1CC1) proteins in the sgControl and indicated gene-KO groups in Nalm6 and Raji cell lines. GAPDH was used as a loading control. (F) Western blotting showing the expression levels of LC3B proteins in the sgControl and indicated gene-KO groups in Nalm6 and Raji cell lines. GAPDH was used as a loading control. (G-H) Representative images of LC3B immunofluorescent staining of Nalm6 and Raji cells with sgControl and indicated gene-KO. Number of LC3B puncta per cell was compared between the groups ($n = 6$). Values are shown as the mean ± SD. Differences among groups were calculated with one-way ANOVA tests. (I-J) Flow cytometry showing the level of CD19 expression in negative control, sgControl and indicated gene-KO Nalm6 and Raji cell lines. (K) Cytotoxic analysis of sgControl and indicated gene^{KO} Nalm6 and Raji cells co-cultured with CD19 CAR-T cells (E:T ratio = 1:4) at 37 °C for 24 hours ($n = 3$). Values are shown as the mean ± SD. Statistical differences are calculated with one-way ANOVA with tests. *$P < 0.05$; **$P < 0.01$; ***$P < 0.001$; ****$P < 0.0,001$; ns: not significant.
Abbreviations: ANOVA analysis of variance; CAR-T chimeric antigen receptor T; E:T effector: target; KO knockout; ns: not significant; SD standard deviation; sgRNA single-guide RNA.

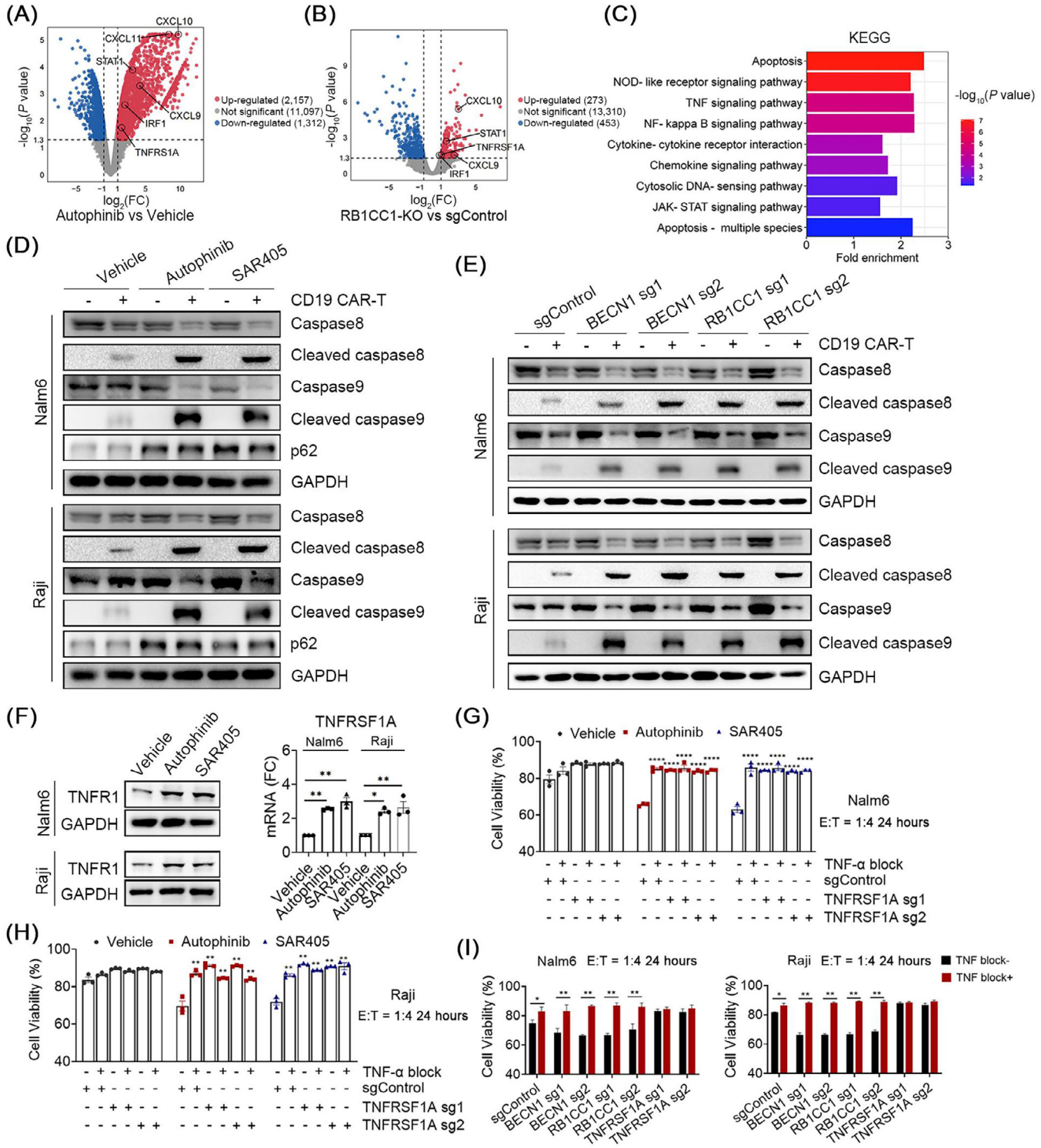

FIGURE 3 Autophagy limits CAR-T cell-mediated cytotoxicity by suppressing TNF-α induced apoptosis. (A) Volcano plot showing varied genes in Nalm6 cells with the addition of vehicle (as control) and autophinib ($\log_2$FC > 1 and $P < 0.05$). (B) Volcano plot showing varied genes between sgControl and indicated RB1CC1^{KO} Nalm6 cells ($\log_2$FC > 1 and $P < 0.05$). (C) KEGG pathway enrichment analysis of varied genes identified in RNA sequencing for Nalm6 cells treated with vehicle (as control) and autophinib. (D) Western blotting showing the expression levels of Caspase-8, Cleaved caspase-8, Caspase-9, Cleaved caspase-9 and p62 proteins after the addition of vehicle (as control), autophinib and SAR405 in Nalm6 and Raji cells when co-cultured with or without CD19 CAR-T cells. GAPDH was used as a loading control. (E) Western blotting showing the expression levels of Caspase-8, Cleaved caspase-8, Caspase-9, Cleaved caspase-9 and p62 proteins in sgControl and indicated gene-KO (sgBECN1, sgRB1CC1) Nalm6 and Raji cells when co-cultured with or without CD19 CAR-T cells. GAPDH was used as a loading control. (F) Expression of TNFRSF1A mRNA by RT-qPCR and TNFR1 protein by western blotting in Nalm6 and Raji

these cells were transfected with STAT1 shRNA (Supplementary Figure S8G-J), suggesting that pharmacological inhibition of autophagy could lead to STAT1-dependent TNFR1 induction. We also detected the secretion of five cytokines from CAR-T cells, including IL-2, IL-6, IL-10, IFN-γ and TNF-α (Supplementary Figure S9A-F). The inhibition of the autophagic activity in cancer cells increased the secretion of only TNF-α from CAR-T cells after co-culture for 24 hours with either cancer cell line at an E:T ratio of 1:1 (Supplementary Figure S9B). Furthermore, the secretion of TNF-α was not affected when CAR-T cells were co-cultured with tumor cells at a low E:T ratio (Supplementary Figure S9B). This finding may be explained by the reason that CAR-T cells require the stimulation of tumor cells during co-culture to produce and secrete cytokines, which would be promoted by inhibiting the autophagic activity of tumor cells before the co-culture. We next observed that TNF-α secreted by CAR-T cells dropped after co-culture for 48 hours (Supplementary Figure S9G), possibly indicating that TNF-α was consumed through binding to the TNF receptor, consistent with the upregulation of TNFR1 observed after autophagy inhibition (Figure 3F). Moreover, the flow cytometry assay showed that both $CD4^+$ T and $CD8^+$ CAR-T cells were responsible for the production of TNF-α (Supplementary Figure S9H). Next, the tumor cell-killing assay showed that the additional treatment with a TNF-α blocking antibody or the knockout of TNFRSF1A significantly decreased cancer cell sensitity to CAR-T cells even in the presence of pre-treatment with autophinib or SAR405 (Figure 3G-H). To further determine whether autophagy regulated the cancer cell sensitivity to CAR-T cell immunotherapy through TNF-α-induced apoptosis, we tested the effect of TNF blocking in the context of knockout of autophagy-related genes (Figure 3I). As expected, the knockout of RB1CC1 or BECN1 could increase the cancer cell sensitivity to CAR-T cells, but this sensitization effect could be attenuated by TNF blocking (Figure 3I). To conclude, the findings indicate that TNF-α-TNFR1 signaling is an important contributor to the autophagy-mediated resistance of cancer cells to CAR-T cells.

3.4 | Autophagy inhibitors suppress tumor growth and reprogram the tumor microenvironment (TME) in mice

To evaluate the impact of pharmacological targeting of autophagy on tumor growth and tumor weight in a mouse model, two selective autophagy inhibitors were used: autophinib and SAR405 (Figure 4A). Systemic treatment of mice bearing tumors formed from A20 cells (a murine lymphoma cell line) with autophinib and SAR405 resulted in significant inhibition of tumor growth and a reduction in tumor weight (Figure 4B-D). We then investigated whether this autophagy-dependent anti-tumor activity was associated with the modulation of the tumor immune landscape. Comprehensive immunophenotyping of different immune cell subpopulations was performed by flow cytometry to identify and quantify both immune effector and immune suppressor cell subsets infiltrating into A20 tumors. The gating strategies used for immunophenotyping are presented in Supplementary Figure S10A-C. The infiltration of $CD3^+$ T, $CD8^+$ T, Th1 and NK cells was increased in A20 tumors treated with either autophinib or SAR405, and the infiltration of immunosuppressive subset myeloid-derived suppressor cells (MDSCs), regulatory T cells and M2-type macrophages were decreased (Figure 4E). However, the composition and distribution of immune cells in the bone marrow were not significantly affected by autophagy inhibitors (Figure 4F). Furthermore, the expression of CD69, PD-1 and TIM-3 in $CD4^+$ T and $CD8^+$ T cells showed no significant difference among the three groups (Figure 4G-H). The increased infiltration of $CD3^+$ T cells into A20 tumors in the three groups was also immunohistochemically verified on three different tumor sections, and the infiltration of $F4/80^+$ macrophages did not differ significantly (Figure 4I-J). As apoptosis was previously found to be a core pathway involved in CAR-T cell resistance, we also detected the level of cleaved-caspase9 in A20 tumors by IHC. The higher expression of cleaved caspase9 in A20 tumors treated with autophinib and/or SAR405 indicated an increase in cell apoptosis (Figure 4I-J).

cells after addition of vehicle (as control), autophinib and SAR405 ($n = 3$). Values are shown as the mean ± SD. Statistical differences among three groups in each cell line are calculated with one-way ANOVA with tests. (G-H) Cytotoxic analysis of sgControl and indicated gene-KO (sgTNFRSF1A) Nalm6 and Raji cells co-cultured with CD19 CAR-T cells (E:T ratio = 1:4) when treated with vehicle (as control), autophinib and SAR405 and then with or without TNF-block ($n = 3$). Values are shown as the mean ± SD. Statistical differences are calculated with two-way ANOVA with tests. (I) Cytotoxic analysis of sgControl and indicated gene-KO (sgBECN1, sgRB1CC1, sgTNFRSF1A) Nalm6 and Raji cells co-cultured with CD19 CAR-T cells (E: T ratio = 1: 4) when treated with or without TNF block ($n = 3$). Values are shown as the mean ± SD. Statistical differences are calculated with two-way ANOVA with tests. *$P < 0.05$; **$P < 0.01$; ***$P < 0.001$; ****$P < 0.0,001$; ns: not significant. Abbreviations: ANOVA analysis of variance; CAR-T chimeric antigen receptor T; E:T effector:target; FC fold change; FC fold change; KO knockout; KEGG Kyoto Encyclopedia of Genes and Genomes; RT-qPCR real-time quantitative polymerase chain reaction; ns: not significant; SD standard deviation; sg single guide; TNF tumor necrosis factor; TNFR1 tumor necrosis factor receptor 1.

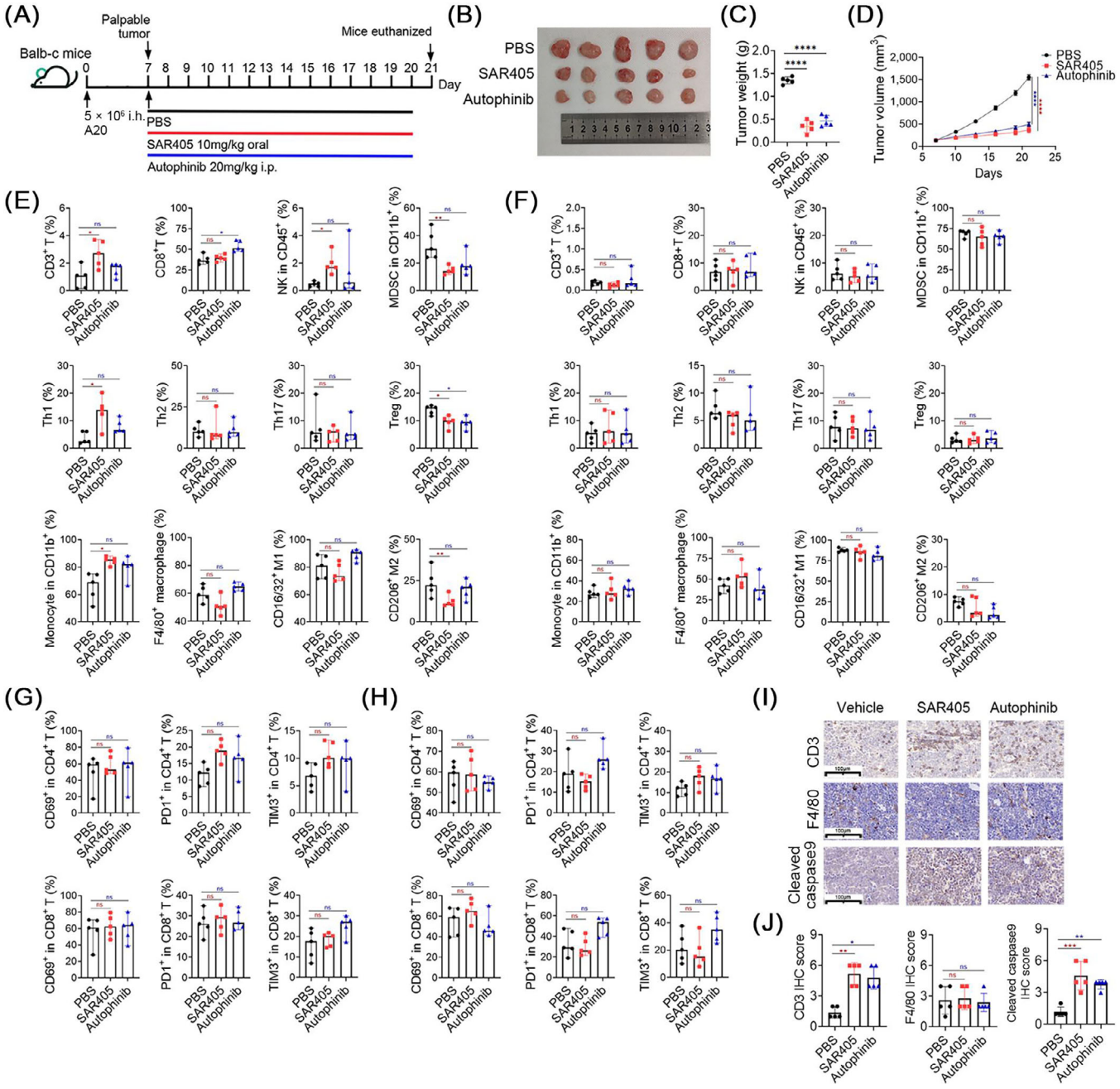

FIGURE 4 Autophagy targeting suppresses tumor growth and promotes T cell infiltration in mice. (A) Schematic of in vivo experiment to evaluate the impact of vehicle (as control), autophinib and SAR405 on tumor growth and tumor weight in A20 B-cell lymphoma mouse model (Balb-c mice, $n = 5$). (B-C) Representative tumor images and weight in grams in A20 tumor-bearing mice treated with PBS (control), SAR405 or autophinib. Values are shown as the mean ± SD. Differences among groups were calculated with one-way ANOVA tests. (D) Tumor growth curves in A20 tumor-bearing mice treated with PBS (control), SAR405 or autophinib. Values are shown as the mean ± SD. Differences among groups were calculated with two-way ANOVA tests. (E-F) Flow cytometry quantification of various immune cell subsets infiltrating in A20 tumors and bone marrow when treated with PBS (control), SAR405 or autophinib. Values are shown as the median with range. Differences among groups were calculated with the Kruskal–Wallis test. (G-H) Flow cytometry quantification of the expression of CD69, PD-1 and TIM3 in $CD4^+$ T and $CD8^+$ T cells infiltrating in A20 tumors and bone marrow when treated with PBS (control), SAR405 or autophinib. Values are shown as the median with range. Differences among groups were calculated with the Kruskal–Wallis test. (I-J) IHC staining on tumor sections showing the expression of CD3, F4/80 and Cleaved-caspase9 proteins. Scale bar: 100 μm. Values are shown as the mean ± SD. Statistical differences are calculated with one-way ANOVA tests. *$P < 0.05$; **$P < 0.01$; ***$P < 0.001$; ****$P < 0.0,001$; ns: not significant. Abbreviations: ANOVA analysis of variance; i.h. hypodermic injection; i.p. intraperitoneal injection; IHC immunohistochemistry staining; MDSCs myeloid-derived suppressor cells; NK natural killer; ns: not significant. PBS phosphate buffer solution; SD standard deviation; Th T helper; Tregs regulatory T cells.

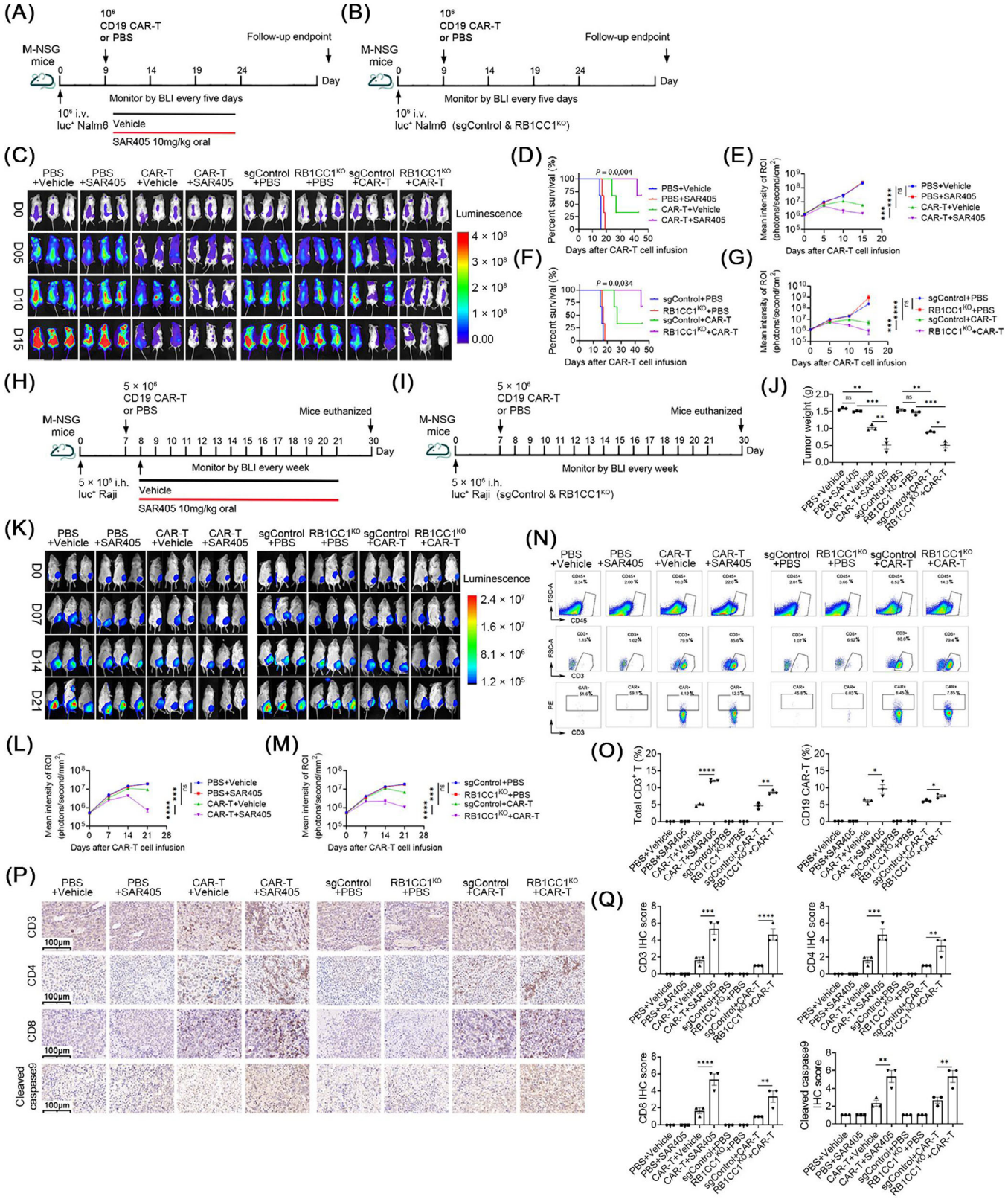

FIGURE 5 Autophagy targeting improves CAR-T cell killing in leukemia and lymphoma mouse models. (A-B) Schematic of in vivo experiment to evaluate the impact of autophagy targeting in luc$^+$ Nalm6 leukemia-bearing M-NSG mouse model ($n = 3$). (C-E) Leukemia progression was evaluated by bioluminescence imaging and quantitated by mean intensity among groups: i) mice inoculated with luc$^+$ Nalm6 cells treated with vehicle alone, SAR405 alone, the combination of vehicle and CD19 CAR-T cells, and combination of SAR405 and CD19 CAR-T cells; ii) mice inoculated with luc$^+$ Nalm6 cells treated with sgControl or RB1CC1^{KO} Nalm6 cells and treated with or without CD19 CAR-T cells. Values are shown as the mean ± SD. Statistical differences among groups were calculated with two-way ANOVA tests. (F-G) As

3.5 | Targeting autophagy enhances CAR-T-cell-mediated killing in leukemia and lymphoma mouse models

We further investigated the effect of autophagy signaling on the anti-tumor activity of CD19 CAR-T cells in vivo (Figure 5A-B). We first engrafted M-NSG mice with luc$^+$ Nalm6 cells and then delivered CD19 CAR-T cells with or without autophagy targeting. Although the results of in vitro cytotoxicity assays showed that the resistance to CD19 CAR-T-driven killing was suppressed, we also observed inhibition of tumor growth and improved survival outcomes in CAR-T-treated mice with the treatment of SAR405 (Figure 5C-E). Furthermore, mice engrafted with RB1CC1^{KO} luc$^+$ Nalm6 cells demonstrated higher sensitivity to CD19 CAR-T-mediated killing in vivo (Figure 5C, F-G). We evaluated the anti-tumor activity of CD19 CAR-T cells with or without autophagy inhibition in a lymphoma mouse model (Figure 5H-I). Consistent with the findings in the leukemia mouse model, tumor growth was suppressed and tumor weight was reduced upon CD19 CAR-T cell infusion when combined with SAR405 treatment or knockout of RB1CC1 in luc$^+$ Raji cells (Figure 5J-M). Remarkably, the flow cytometry assays confirmed the increased infiltration of total CD3$^+$ T and CD19 CAR-T cells into luc$^+$ Raji tumors when treated with SAR405 or knockout of RB1CC1 in luc$^+$ Raji cells (Figure 5N-O). IHC staining of tumor sections also demonstrated higher infiltration of total CD3$^+$ T, CD4$^+$ T and CD8$^+$ T cells and elevated apoptosis after either SAR405 treatment or knockout of RB1CC1 (Figure 5P-Q). Thus, it could be hypothesized that both the increased lymphocyte infiltration and activated apoptosis might contribute to the enhanced response to CAR-T cell therapy in these tumor models with autophagy impairment. The autophagic activity in tumor cells was reduced more obviously than that in CAR-T cells after the treatment with SAR405 (Supplementary Figure S11A), indicating that the dose of SAR405 used in the animal experiments showed a more pronounced effect on tumor cells. Moreover, genetic knockout of RB1CC1 of tumor cells did not affect the autophagic activity in CAR-T cells (Supplementary Figure S11B). Additionally, treatment with SAR405 did not affect the expression of PD-1 and CD69 in CAR-T cells (Supplementary Figure S11C-D). Therefore, the enhanced anti-tumor effects may result predominantly from inhibition of autophagy in tumor cells. Together, these findings confirmed that autophagy signaling is highly necessary for the anti-tumor effects of CAR-T cells and that disruption of autophagy signaling in B-cell malignancies guards against resistance to CD19 CAR-T cells.

3.6 | Targeting autophagy enhances the chemotactic ability of CAR-T cells via STAT1/IRF1 axis-mediated upregulation of CXCL10 and CXCL11

The chemotactic ability of CAR-T cells was consistently improved in vitro after treatment with the culture supernatants of tumor cells with autophinib treatment or knockout of RB1CC1 (Figure 6A-B), consistent with the increased infiltration observed in mice. Our previous RNA sequencing and GSEA pathway enrichment analyses showed that the differentially-expressed genes between autophagy-targeting Nalm6 cells and control Nalm6 cells were overrepresented mainly in the cytokine-cytokine receptor interaction, chemokine signaling and cytosolic DNA sensing pathways (Figure 6C-E). Of note, three chemokines, namely, CXCL9, CXCL10 and CXCL11, demonstrated marked differential expression, which was also observed in RB1CC1^{KO} or autophinib-treated Nalm6 cells when compared with their control cells (Figure 3A-B). Increased mRNA and protein levels of CXCL10 and

for survival analysis, Log-rank tests were used to analyze the statistical differences between four groups. (H-I) Schematic of in vivo experiment to evaluate the impact of autophagy targeting in luc$^+$ Raji lymphoma-bearing M-NSG mouse model ($n = 3$). (J) Lymphoma progression was evaluated by tumor weight. Values are shown as the mean ± SD. Differences among groups were calculated with one-way ANOVA tests. (K-M) Lymphoma progression was evaluated by bioluminescence imaging and quantitated by mean intensity among groups: i) mice inoculated with luc$^+$ Raji cells treated with vehicle alone, SAR405 alone, the combination of vehicle and CD19 CAR-T cells, and combination of SAR405 and CD19 CAR-T cells; ii) mice inoculated with luc$^+$ Raji cells treated with sgControl or RB1CC1^{KO} Raji cells and treated with or without CD19 CAR-T cells. Values are shown as the mean ± SD. Statistical differences among groups were calculated with one-way ANOVA tests. (N-P) Flow cytometry quantification of total CD3$^+$ T and CD19 CAR-T cells infiltrating in Raji tumors. Values are shown as the mean ± SD. Statistical differences are calculated with one-way ANOVA tests. (Q) IHC staining on tumor sections showing the expression of CD3, CD4, CD8 and Cleaved-caspase9 proteins. Scale bar: 100 μm. (R-U) IHC scores of CD3, CD4, CD8 and cleaved-caspase9 proteins in Raji-tumor samples. Values are shown as the mean± SD. Statistical differences are calculated with one-way ANOVA with tests. *$P < 0.05$; **$P < 0.01$; ***$P < 0.001$; ****$P < 0.0,001$; ns: not significant. Abbreviations: ANOVA analysis of variance; CAR-T chimeric antigen receptor T; i.h. hypodermic injection; i.v. intravenous injection; IHC immunohistochemistry; KO knockout; luc$^+$ luciferase positive; BLI bioluminescence imaging; ns: not significant; PBS phosphate buffer solution; ROI region of Interest; SD standard deviation; sg single guide.

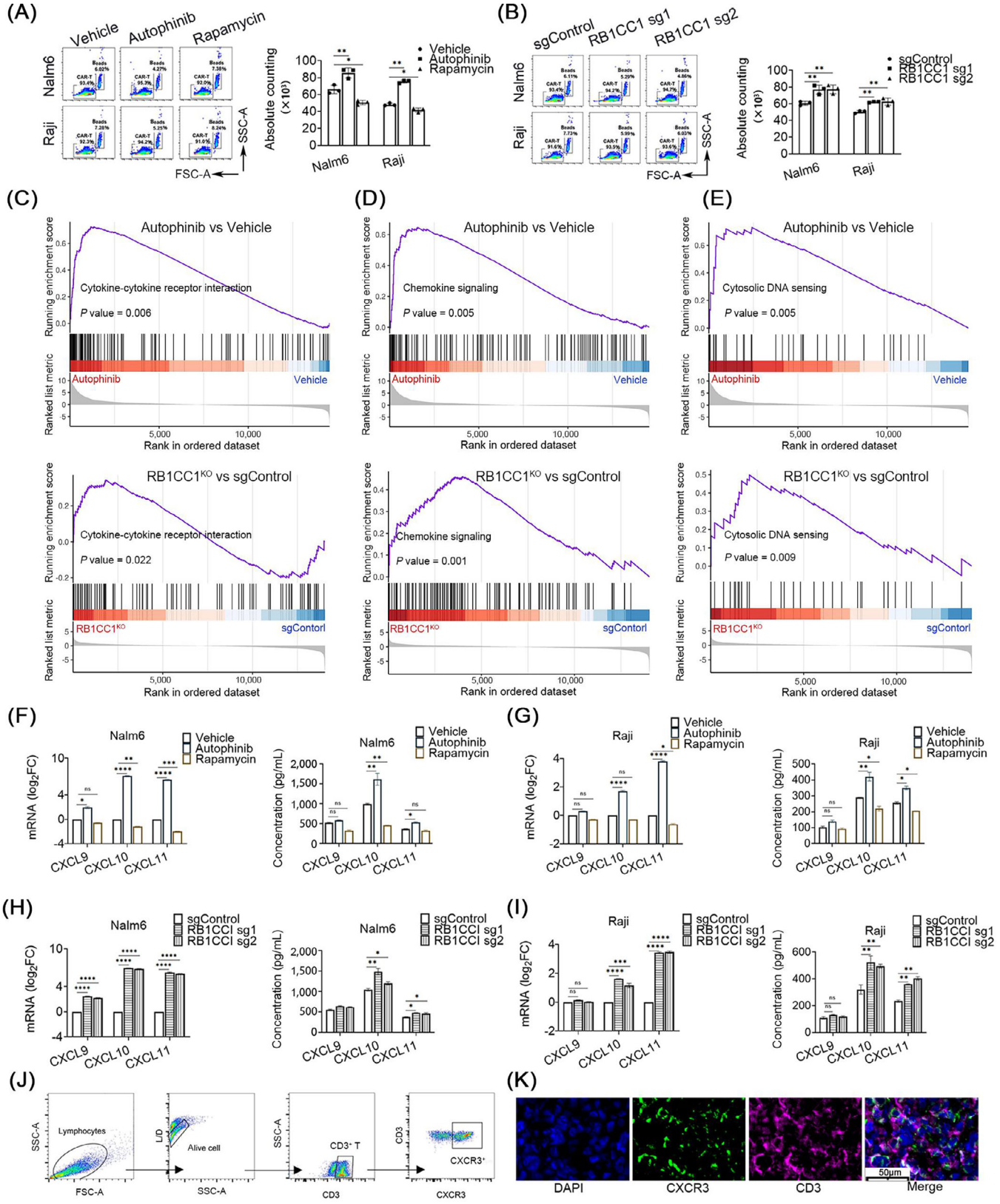

FIGURE 6 Inhibition of autophagy enhances the chemotaxis ability of CAR-T cells by promoting the production and secretion of CXCL10 and CXCL11. (A-B) Chemotaxis assay and cell counting by flow cytometry showing the chemotaxis ability of CD19 CAR-T cells with pharmacological targeting of autophagy and knockout of RB1CC1 in Nalm6 and Raji cells in vitro ($n = 3$). Values are shown as the mean ± SD. Statistical differences between three groups in each cell line are calculated with one-way ANOVA tests. (C-E) GSEA analysis of the most differentially expressed genes between Nalm6 cells treated with vehicle and autophinib for 72 hours. (F-G) Expression of CXCL9, CXCL10 and

CXCL11 were found after pharmacological and genetic inhibition of autophagy (Figure 6F-I). CXCL9, CXCL10 and CXCL11 regulate the activation, differentiation and migration of immune cells via the CXCR3-dependent pathway and trigger immune responses by recruiting immune cells. The high proportion of $CXCR3^+$ CAR-T cells, both in vitro and in vivo, indicated that CXCL10 and CXCL11 play important roles in CAR-T cell recruitment (Figure 6J-K). STAT1-IRF regulatory modules are overrepresented in the promoters of many genes encoding proteins in the inflammatory signature, including chemokines [37]. To further explore the regulatory mechanisms-, we assessed the protein levels of IRF family members based on RNA sequencing data. As shown in Supplementary Figure S12A, we observed that protein levels of IRF1 were elevated in both Nalm6 and Raji cells when treated with autophinib and SAR405. By analysis of ChIP-seq datasets in ChIP-Atlas, we found that STAT1 and IRF1 had binding peaks in the promoter region of CXCL10 and CXCL11 (Supplementary Figure S12B-C). In addition, the protein levels of pSTAT1 and IRF1 were up-regulated after autophagy targeting (Figure 7A-B). To establish a direct relationship between the activation of the STAT1/IRF1 axis and the expression of chemokines, we knocked down STAT1 or IRF1 (Supplementary Figure S13A-B) in cells pre-treated with autophinib or SAR405 and analyzed the chemotactic ability (Supplementary Figure S13C-D). The chemotactic ability of CD19 CAR-T cells was suppressed after treatment with the culture supernatants of Nalm6 and Raji cells with knockdown of STAT1 and IRF1 (Supplementary Figure S13C-D). Moreover, IRF1 induction was no longer observed in both autophagy inhibitor-treated Nalm6 and Raji cells when pre-transfected with STAT1 shRNA (Figure 7C-D). Autophinib and SAR405 failed to induce CXCL10 and CXCL11 mRNA and protein expression *in vitro* in the absence of STAT1 or IRF1 (Figure 7E-F). The ChIP-qPCR results further validated the binding of STAT1 and IRF1 to the promoter region of CXCL10 and CXCL11 (Figure 7G-H). Our study showed that pharmacological inhibition of autophagy promoted the accumulation of cytosolic DNA (Supplementary Figure S13E-F). It has been reported that autophagy could inhibit type I IFN secretion by irradiated cancer cells as a consequence of improved cytosolic DNA clearance, thereby increasing the sensitivity of mouse mammary carcinoma cells to radiation therapy [38]. When the IFN signaling pathway is activated, STAT1 protein is phosphorylated by its kinase JAK1 and then forms heterodimers or homodimers that translocate to the nucleus to regulate the transcriptional activation of downstream target genes [39–41]. Therefore, the inhibition of autophagy may promote the transcription and phosphorylation of STAT1 by accumulation of cytosolic DNA. Moreover, by performing IHC assays, we found that the protein level of pSATA1 was significantly higher in the non-responder group than in the responder group, indicating the negative correlation between pSATA1 expression and clinical response (Supplementary Figure S13G-H). On the basis of these data, we concluded that attenuation of autophagic activity of cancer cells could up-regulate both STAT1 and IRF1 as a consequence of the accumulation of cytosolic DNA, which thereby promoted the expression and secretion of the cytokines CXCL10 and CXCL11.

4 | DISCUSSION

Despite the efficacy of CAR-T cell therapy for a wide array of hematological cancers, some patients still either fail to achieve a response or develop resistance. Primary resistance to CD19 CAR-T cell therapy is an obvious obstacle to the treatment of B-cell malignancies [4]. The mechanisms responsible for the cancer-intrinsic resistance to CAR-T cells have yet to be elucidated to identify new solutions for primary resistance and relapse. In this study, we conducted an unbiased genome-wide loss-of-function screening and found that the enrichment of autophagy-related genes could protect tumor cells against CD19 CAR-T cell-mediated cytotoxicity, indicating the critical importance of autophagy in evasion of CAR-T therapy. The IHC staining results of autophagy-related proteins in tumor samples and bulk RNA sequencing analysis of bone marrow samples

CXCL11 mRNA by RT-qPCR and ELISA quantification of CXCL9, CXCL10 and CXCL11 protein levels in the supernatants of Nalm6 cells and Raji cells with the addition of vehicle (as control), autophinib and SAR405 ($n = 3$). Values are shown as the mean ± SD. Statistical differences are calculated with one-way ANOVA tests. (H-I) Expression of CXCL9, CXCL10 and CXCL11 mRNA by RT-qPCR and ELISA quantification of CXCL9, CXCL10 and CXCL11 protein levels in the supernatants of sgControl and $RB1CC1^{KO}$ Nalm6 and Raji cells ($n = 3$). Values are shown as the mean ± SD. Statistically significant differences are calculated with two-way ANOVA tests. (J) Flow cytometry showing the expression of CXCR3 in CAR-T cells. (K) Immunofluorescent staining on tumor sections showing the expression of CXCR3 in CAR-T cells. Scale bar: 50 μm. *$P < 0.05$; **$P < 0.01$; ***$P < 0.001$; ****$P < 0.0,001$; ns: not significant. Abbreviations: CAR-T chimeric antigen receptor T; CXCL CXC chemokine ligand;ANOVA analysis of variance; ELISA enzyme-linked immunosorbent assay; FC fold change; GSEA gene set enrichment analysis; ns: not significant; PBS phosphate buffer solution; RT-qPCR real-time quantitative polymerase chain reaction; SD standard deviation.

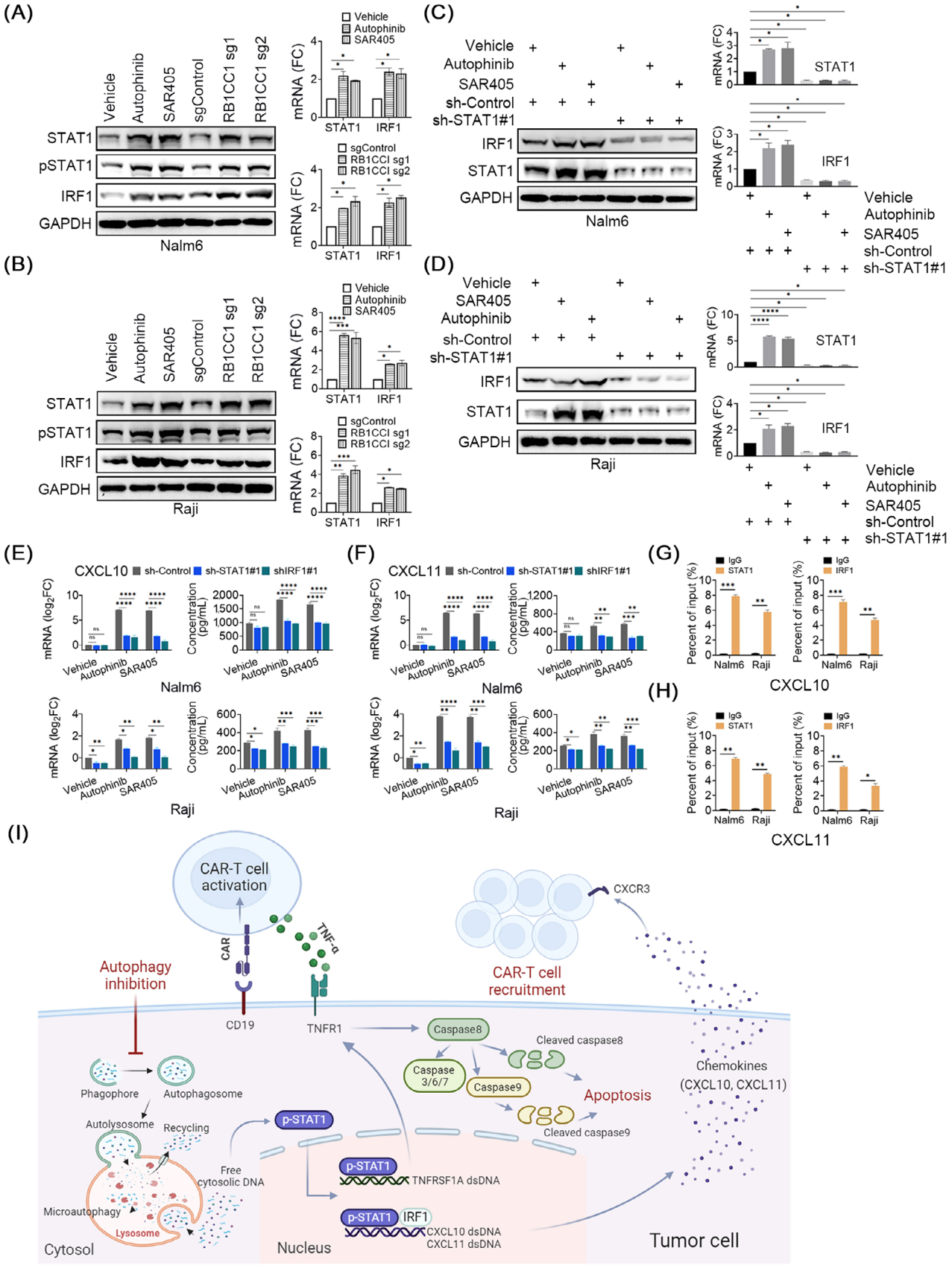

FIGURE 7 STAT1/IRF1 axis mediates the upregulation of CXCL10 and CXCL11 induced by autophagy targeting. (A-B) Western blotting showing the expression levels of STAT1, pSTAT1, and IRF1 proteins in Nalm6 and Raji cells after the addition of autophagy inhibitors or the knockout of RB1CC1 ($n = 3$). GAPDH was used as a loading control. The histograms showing the expression of STAT1 and IRF1 mRNA by

also suggested the clinical relevance of autophagy to the therapeutic response and relapse after CAR-T cell therapy. We further validated this protective role of autophagy in vitro and in mouse models by knocking out the autophagy-related genes and pharmacologically targeting autophagy.

Autophagy is a tightly regulated and stress-induced catabolic pathway in all eukaryotes, during which double-membraned vesicles are formed that engulf cellular targets, including damaged organelles, unfolded proteins and pathogens and delivered them to the lysosome to be digested [31]. Several studies has demonstrated important functions of autophagy and autophagy-related processes in tumor development, maintenance and progression [42, 43]. As a key recycling process in the complex TME, the role of autophagy in anti-tumor immunity has been increasingly appreciated [42, 43]. It has been reported that targeted autophagy ignites immunosuppressive TME by influencing antigen release, antigen presentation, antigen recognition, and immune cell function [44–46]. The previous genome-wide CRISPR screening across a panel of genetically diverse mouse tumor cell lines has demonstrated that autophagy is a conserved mediator of cancer resistance to cytotoxicity induced by CTLs [17]. However, the regulatory role of human cancer-autonomous autophagy in CAR-T cell immunotherapy remains poorly understood. In addition, pancreatic tumor cells transmitted major histocompatibility complex I (MHC-I) molecules into autophagic vacuoles via autophagy-related receptor NBR1, thus impeding antigen presentation and leading to immune escape [47]. As the recognition of tumor cells by CAR-T cells is independent of MHC molecules, the specific mechanism by which autophagy regulates the resistance of B-cell malignancies to CAR-mediated killing has yet to be elucidated. To explain the above observations, our data offer a novel mechanism by which autophagy mediates cancer-intrinsic biological characteristics contributing to the therapeutic failure of CD19 CAR-T cell therapy, wherein both the chemokine signaling activation and TNF-α-TNFR1 axis-induced apoptosis are involved (Figure 7I).

It has been reported that the apoptotic signaling pathway could regulate the anti-tumor immune response after checkpoint blockade in various tumors, suggesting that this pathway may act as a central regulator of anti-tumor responses to distinct modalities of immunotherapy [48–51]. Moreover, the knockout of autophagy-related genes could exacerbate tumor cell apoptosis and liver injury in mice [48, 49]. Previous studies demonstrated that impaired apoptotic signaling molecules in leukemia cells attenuated CAR-T cell cytotoxicity and drive CAR-T cell dysfunction, further supporting the idea that the apoptosis pathway plays an important role in the successful killing of tumor cells by CAR-T cells [23]. However, the mechanism underlying the role of autophagy in CAR-T cell-mediated killing of tumor cells remains unclear. Interestingly, we first revealed that targeting autophagy enhanced the cancer cell sensitivity to CAR-T cell killing through TNF-α-TNFR1-dependent apoptosis. More specifically, inhibition of autophagy could induce the expression of TNFR1, and TNF-α-induced apoptosis could be suppressed when TNFRSF1A was knocked out. The secretion of TNF-α from CAR-T cells would be promoted at an early stage by inhibiting the autophagic activity in tumor cells before the co-culture, and TNF-α was then consumed through binding to the TNF receptor. In addition, autophagy appeared to inhibit the formation and activity of active caspase8 and caspase9, which consequently resulted in suppressed TNF-α-dependent apoptosis. These data indicate that TNF-α-TNFR1 signaling is an important contributor to the autophagy-mediated cancer cell resistance to CAR-T cells. Future studies are warranted to further elucidate the precise molecular mechanisms through which autophagy restricts TNF-α-TNFR1-dependent apoptosis.

RT-qPCR quantification. Values are shown as the mean ± SD. Statistical differences are calculated with one-way ANOVA tests. (C-D) Western blotting showing the expression levels of STAT1 and IRF1 proteins in Nalm6 and Raji cells after the addition of autophagy inhibitors and the silencing of STAT1 ($n = 3$). GAPDH was used as a loading control. The histograms showing the expression of STAT1 and IRF1 mRNA by RT-qPCR quantification. Values are shown as the mean ± SD. Statistical differences are calculated with one-way ANOVA tests. (E-F) Expression of CXCL10 and CXCL11 mRNA by RT-qPCR and ELISA quantification of CXCL10 and CXCL11 protein levels in the supernatants of shControl, shSTAT1 and shIRF1 Nalm6 and Raji cells ($n = 3$). Values are shown as the mean ± SD. Statistical differences are calculated with two-way ANOVA tests. (G-H) ChIP-qPCR showing the binding of STAT1 and IRF1 to the promoter region of CXCL10 and CXCL11 ($n = 3$). Values are shown as the mean ± SD. Statistical differences for each cell line are calculated with unpaired Student's t tests. (I) Graphic abstract: in the proposed model, inhibition of cancer cell-autonomous autophagy leads to accumulation of cytosolic DNA, which thereby not only suppresses cancer cell survival by inducing TNFR1-TNF-α mediated apoptosis but also promotes the CAR-T cell recruitment in tumor microenvironment via STAT1/IRF1-dependent activation of chemokine signaling. *$P < 0.05$; **$P < 0.01$; ***$P < 0.001$; ****$P < 0.0,001$; ns: not significant. Abbreviations: ANOVA analysis of variance; CAR-T, chimeric antigen receptor T; ChIP, chromatin immunoprecipitation; CXCL CXC, chemokine ligand; ELISA, enzyme-linked immunosorbent assay; FC, fold change; IRF, interferon regulatory factor; ns: not significant; RT-qPCR, real-time quantitative polymerase chain reaction; SD, standard deviation; sh short hairpin; STAT, signal transducers and activators of transcription.

As reported, targeting autophagy could inhibit melanoma growth by enhancing NK cell infiltration in a CCL5-dependent manner [52], indicating its utility as a novel therapeutic alternative for improving the efficacy of cancer immunotherapy. The expression of IFN-inducible chemokines was also found to be significantly increased in lungs bearing minimal metastatic lesions and melanoma metastases, and chemokine blockade with specific antibodies inhibited the migration of $CD8^+$ T cells [53, 54]. Therefore, targeting autophagy may lead to inhibition of tumor growth and increased infiltration of cytotoxic immune cells [52, 55-57]. However, whether targeting cancer-intrinsic autophagy could contribute to CAR-T cell recruitment remains to be explored. Notably, our cytokine profiling analysis identified CXCL10 and CXCL11 as two major chemokines upregulated by autophagy inhibition in Nalm6 and Raji cells. Furthermore, our data suggested that CXCL10 and CXCL11 were secreted from tumor cells at least partially in response to autophagy inhibition. The activated STAT1/IRF1 pathway in the transcriptional regulation is involved in the autophagy-related mechanisms underlying the production and secretion of CXCL10 and CXCL11. STAT1 serves as an upstream and is the major inducer of IRF1. Thus, IRF1 induction in cancer cells in pharmacological inhibition of autophagy was significantly abrogated when either STAT1 or IRF1 was silenced. Increased generation of cytosolic DNA fragments occurred along with the inhibition of autophagy, and the extranuclear DNA fragments colocalized with cGAS and activated the cGAS-STING-STAT1 signaling axis [58]. Therefore, the activation of the STAT1/IRF1 pathway after autophagy targeting may be the result of the cytosolic DNA fragment accumulation. To conclude, our data further validated the role of IFN-inducible CXCR3-cognate chemokine activation, induced by autophagy targeting in reversing tumor immune escape.

While our study revealed that disrupting autophagy signaling could enhance cancer sensitivity to CAR-T cell-mediated killing, promising biomarkers for patient selection for CAR-T therapy still have to be identified for further clinical assessment of these findings. In addition, future potent and specific autophagy inhibitors need to be developed and may provide promising strategies for improving the effectiveness of CAR-T therapy. In response to stress signals in the tumor microenvironment, the autophagy pathway is altered in both tumor cells and immune cells, thereby differentially affecting tumor progression, immunity and therapy [31, 45]. Multiple stress signals affect the autophagy-dependent changes in various immune cells, including NK cells, T cells, regulatory T cells and antigen-processing cells (APCs), and could also directly regulate anti-tumor immunity [59–61]. This is another important issue that we should take into account. Interestingly enough, one previous study [61], consistent with our findings, has also reported that anti-tumor adaptive immunity is not adversely impaired by autophagy inhibition in mouse models, suggesting the possibility of combining autophagy inhibitors with immunotherapy in certain clinical contexts.

5 | CONCLUSIONS

In conclusion, this genome-wide CRISPR screening identified autophagy-related genes essential for resistance to CAR-T-mediated killing and showed that either genetic or pharmacological inhibition of autophagy could alter cancer-immune signaling and increase responsiveness to CD19 CAR-T cells. Our findings offer a novel perspective in which targeting cancer-intrinsic autophagy rescues therapeutic failure of CAR-T cell therapy by promoting TNF-α-TNFR1 mediated apoptosis and STAT1/IRF1-induced chemokine signaling activation. These findings might provide a promising basis for "CAR-T + X" combination therapies and contribute to the improvement of the clinical efficacy of CAR-T cell immunotherapy.

DECLARATIONS

AUTHOR CONTRIBUTIONS

Study concept and experimental design: Lu Tang, Heng Mei, Yu Hu; Conducting experiments: Lu Tang, Huan Zhang, Wenjing Luo, Xindi Wang, Jie Zhou; Data analysis and interpretation: Lu Tang, Huan Zhang, Fen Zhou, Mengyi Du, Zhaozhao Chen, Jianghua Wu, Chenggong Li, Yinqiang Zhang, Wei Xiong; Supervision: Fen Zhou, Yuxi Wen, Jianghua Wu, Zhuolin Wu, Qiuzhe Wei, Haiming Kou, Zhongpei Huang, Danying Liao, Huiwen Jiang; Writing—original draft: Lu Tang, Huan Zhang, Heng Mei; Writing—review & editing: Lu Tang, Heng Mei, Yu Hu; All authors contributed to reading and editing the manuscript. The corresponding authors are responsible for all aspects of this work.

ETHICS APPROVAL AND CONSENT TO PARTICIPATE

Tumor tissue samples before CD19 CAR-T cell infusion were obtained from patients with B-cell lymphoma in a clinical trial (NCT04008251, "Treatment of Relapsed or Refractory B-cell Malignancies by Humanized CD19 Chimeric Antigen Receptor (CAR)-Modified T Cells"). The study obtained informed consent from all participants and was approved by the Ethics Committee of the Union Hospital affiliated with Huazhong University of Science and Technology, Wuhan, China (REC ref no. [2019]008). All

in vivo animal experiments were approved by the Ethics Committee of Tongji Medical College, Huazhong University of Science and Technology (IACUC No. 2727), Wuhan, China.

CONSENT FOR PUBLICATION

Not applicable.

CONFLICT OF INTEREST STATEMENT

No potential conflicts of interest were disclosed.

AVAILABILITY OF DATA AND MATERIALS

All datasets generated or analyzed during this study have been included in this manuscript. The data are available from the corresponding author on reasonable request.

ACKNOWLEDGMENTS

We thank all authors for their contribution to this work. We thank the technical support from Analytical & Testing Center, Medical sub-center, Huazhong University of Science & Technology, Wuhan China. This work was supported by grants from the National Key R & D Program of China (2022YFC2502700), the National Natural Science Foundation of China (No. 81873434; No. 82100190; No.82200145), and the China Postdoctoral Innovative Talent Support Foundation (No. BX2021106).

ORCID

Jianghua Wu https://orcid.org/0000-0001-8862-4069
Heng Mei https://orcid.org/0000-0001-7941-2443

REFERENCES

1. Salter AI, Pont MJ, Riddell SR. Chimeric antigen receptor-modified T cells: CD19 and the road beyond. Blood. 2018;131(24):2621-9.
2. Maude SL, Laetsch TW, Buechner J, Rives S, Boyer M, Bittencourt H, et al. Tisagenlecleucel in Children and Young Adults with B-Cell Lymphoblastic Leukemia. N Engl J Med. 2018;378(5):439-48.
3. Park JH, Rivière I, Gonen M, Wang X, Sénéchal B, Curran KJ, et al. Long-Term Follow-up of CD19 CAR Therapy in Acute Lymphoblastic Leukemia. N Engl J Med. 2018;378(5):449-59.
4. Larson RC, Maus MV. Recent advances and discoveries in the mechanisms and functions of CAR T cells. Nat Rev Cancer. 2021;21(3):145-61.
5. Fraietta JA, Lacey SF, Orlando EJ, Pruteanu-Malinici I, Gohil M, Lundh S, et al. Determinants of response and resistance to CD19 chimeric antigen receptor (CAR) T cell therapy of chronic lymphocytic leukemia. Nat Med. 2018;24(5):563-71.
6. Orlando EJ, Han X, Tribouley C, Wood PA, Leary RJ, Riester M, et al. Genetic mechanisms of target antigen loss in CAR19 therapy of acute lymphoblastic leukemia. Nat Med. 2018;24(10):1504-6.
7. Sotillo E, Barrett DM, Black KL, Bagashev A, Oldridge D, Wu G, et al. Convergence of Acquired Mutations and Alternative Splicing of CD19 Enables Resistance to CART-19 Immunotherapy. Cancer Discov. 2015;5(12):1282-95.
8. Ledererova A, Dostalova L, Kozlova V, Peschelova H, Ladungova A, Culen M, et al. Hypermethylation of CD19 promoter enables antigen-negative escape to CART-19 in vivo and in vitro. J Immunother Cancer. 2021;9(8):e002352.
9. Chen J, López-Moyado IF, Seo H, Lio CJ, Hempleman LJ, Sekiya T, et al. NR4A transcription factors limit CAR T cell function in solid tumours. Nature. 2019;567(7749):530-4.
10. Cherkassky L, Morello A, Villena-Vargas J, Feng Y, Dimitrov DS, Jones DR, et al. Human CAR T cells with cell-intrinsic PD-1 checkpoint blockade resist tumor-mediated inhibition. J Clin Invest. 2016;126(8):3130-44.
11. Gulati P, Rühl J, Kannan A, Pircher M, Schuberth P, Nytko KJ, et al. Aberrant Lck Signal via CD28 Costimulation Augments Antigen-Specific Functionality and Tumor Control by Redirected T Cells with PD-1 Blockade in Humanized Mice. Clin Cancer Res. 2018;24(16):3981-93.
12. Rafiq S, Yeku OO, Jackson HJ, Purdon TJ, van Leeuwen DG, Drakes DJ, et al. Targeted delivery of a PD-1-blocking scFv by CAR-T cells enhances anti-tumor efficacy in vivo. Nat Biotechnol. 2018;36(9):847-56.
13. Shah NN, Fry TJ. Mechanisms of resistance to CAR T cell therapy. Nat Rev Clin Oncol. 2019;16(6):372-85.
14. Joung J, Konermann S, Gootenberg JS, Abudayyeh OO, Platt RJ, Brigham MD, et al. Genome-scale CRISPR-Cas9 knockout and transcriptional activation screening. Nat Protoc. 2017;12(4):828-63.
15. Shalem O, Sanjana NE, Hartenian E, Shi X, Scott DA, Mikkelson T, et al. Genome-scale CRISPR-Cas9 knockout screening in human cells. Science. 2014;343(6166):84-7.
16. Neff EP. CRISPR takes genetic screens forward. Lab Anim (NY). 2020;49(1):13-6.
17. Lawson KA, Sousa CM, Zhang X, Kim E, Akthar R, Caumanns JJ, et al. Functional genomic landscape of cancer-intrinsic evasion of killing by T cells. Nature. 2020;586(7827):120-6.
18. Manguso RT, Pope HW, Zimmer MD, Brown FD, Yates KB, Miller BC, et al. In vivo CRISPR screening identifies Ptpn2 as a cancer immunotherapy target. Nature. 2017;547(7664):413-8.
19. Hart T, Chandrashekhar M, Aregger M, Steinhart Z, Brown KR, MacLeod G, et al. High-Resolution CRISPR Screens Reveal Fitness Genes and Genotype-Specific Cancer Liabilities. Cell. 2015;163(6):1515-26.
20. Liu D, Zhao X, Tang A, Xu X, Liu S, Zha L, et al. CRISPR screen in mechanism and target discovery for cancer immunotherapy. Biochim Biophys Acta Rev Cancer. 2020;1874(1):188378.
21. Patel SJ, Sanjana NE, Kishton RJ, Eidizadeh A, Vodnala SK, Cam M, et al. Identification of essential genes for cancer immunotherapy. Nature. 2017;548(7669):537-42.
22. Larson RC, Kann MC, Bailey SR, Haradhvala NJ, Llopis PM, Bouffard AA, et al. CAR T cell killing requires the IFNγR pathway in solid but not liquid tumours. Nature. 2022;604(7906):563-70.
23. Singh N, Lee YG, Shestova O, Ravikumar P, Hayer KE, Hong SJ, et al. Impaired Death Receptor Signaling in Leukemia Causes Antigen-Independent Resistance by Inducing CAR T-cell Dysfunction. Cancer Discov. 2020;10(4):552-67.
24. Dufva O, Koski J, Maliniemi P, Ianevski A, Klievink J, Leitner J, et al. Integrated drug profiling and CRISPR screening

identify essential pathways for CAR T-cell cytotoxicity. Blood. 2020;135(9):597-609.
25. Li W, Xu H, Xiao T, Cong L, Love MI, Zhang F, et al. MAGeCK enables robust identification of essential genes from genome-scale CRISPR/Cas9 knockout screens. Genome Biol. 2014;15(12):554.
26. Rajabzadeh A, Hamidieh AA, Rahbarizadeh F. Spinoculation and retronectin highly enhance the gene transduction efficiency of Mucin-1-specific chimeric antigen receptor (CAR) in human primary T cells. BMC Mol Cell Biol. 2021;22(1):57.
27. Subramanian A, Tamayo P, Mootha VK, Mukherjee S, Ebert BL, Gillette MA, et al. Gene set enrichment analysis: a knowledge-based approach for interpreting genome-wide expression profiles. Proc Natl Acad Sci U S A. 2005;102(43):15545-50.
28. Bustin SA, Benes V, Garson JA, Hellemans J, Huggett J, Kubista M, et al. The MIQE guidelines: minimum information for publication of quantitative real-time PCR experiments. Clin Chem. 2009;55(4):611-22.
29. Galluzzi L, Green DR. Autophagy-Independent Functions of the Autophagy Machinery. Cell. 2019;177(7):1682-99.
30. Gatica D, Lahiri V, Klionsky DJ. Cargo recognition and degradation by selective autophagy. Nat Cell Biol. 2018;20(3):233-42.
31. Xia H, Green DR, Zou W. Autophagy in tumour immunity and therapy. Nat Rev Cancer. 2021;21(5):281-97.
32. Kearney CJ, Vervoort SJ, Hogg SJ, Ramsbottom KM, Freeman AJ, Lalaoui N, et al. Tumor immune evasion arises through loss of TNF sensitivity. Sci Immunol. 2018;3(23):eaar3451.
33. Vredevoogd DW, Kuilman T, Ligtenberg MA, Boshuizen J, Stecker KE, de Bruijn B, et al. Augmenting Immunotherapy Impact by Lowering Tumor TNF Cytotoxicity Threshold. Cell. 2019;178(3):585-99.e15.
34. Mariño G, Niso-Santano M, Baehrecke EH, Kroemer G. Self-consumption: the interplay of autophagy and apoptosis. Nat Rev Mol Cell Biol. 2014;15(2):81-94.
35. Martínez-Lostao L, Anel A, Pardo J. How Do Cytotoxic Lymphocytes Kill Cancer Cells? Clin Cancer Res. 2015;21(22):5047-56.
36. Bertheloot D, Latz E, Franklin BS. Necroptosis, pyroptosis and apoptosis: an intricate game of cell death. Cell Mol Immunol. 2021;18(5):1106-21.
37. Sikorski K, Wesoly J, Bluyssen HA. Data mining of atherosclerotic plaque transcriptomes predicts STAT1-dependent inflammatory signal integration in vascular disease. Int J Mol Sci. 2014;15(8):14313-31.
38. Yamazaki T, Kirchmair A, Sato A, Buqué A, Rybstein M, Petroni G, et al. Mitochondrial DNA drives abscopal responses to radiation that are inhibited by autophagy. Nat Immunol. 2020;21(10):1160-71.
39. González-Navajas JM, Lee J, David M, Raz E. Immunomodulatory functions of type I interferons. Nat Rev Immunol. 2012;12(2):125-35.
40. Ivashkiv LB, Donlin LT. Regulation of type I interferon responses. Nat Rev Immunol. 2014;14(1):36-49.
41. Hu X, Ivashkiv LB. Cross-regulation of signaling pathways by interferon-gamma: implications for immune responses and autoimmune diseases. Immunity. 2009;31(4):539-50.
42. Debnath J, Gammoh N, Ryan KM. Autophagy and autophagy-related pathways in cancer. Nat Rev Mol Cell Biol. 2023:1-16.
43. Jiang T, Chen X, Ren X, Yang JM, Cheng Y. Emerging role of autophagy in anti-tumor immunity: Implications for the modulation of immunotherapy resistance. Drug Resist Updat. 2021;56:100752.
44. Jin Z, Sun X, Wang Y, Zhou C, Yang H, Zhou S. Regulation of autophagy fires up the cold tumor microenvironment to improve cancer immunotherapy. Front Immunol. 2022;13:1018903.
45. Poillet-Perez L, Sarry JE, Joffre C. Autophagy is a major metabolic regulator involved in cancer therapy resistance. Cell Rep. 2021;36(7):109528.
46. Katheder NS, Khezri R, O'Farrell F, Schultz SW, Jain A, Rahman MM, et al. Microenvironmental autophagy promotes tumour growth. Nature. 2017;541(7637):417-20.
47. Yamamoto K, Venida A, Yano J, Biancur DE, Kakiuchi M, Gupta S, et al. Autophagy promotes immune evasion of pancreatic cancer by degrading MHC-I. Nature. 2020;581(7806):100-5.
48. Amir M, Zhao E, Fontana L, Rosenberg H, Tanaka K, Gao G, et al. Inhibition of hepatocyte autophagy increases tumor necrosis factor-dependent liver injury by promoting caspase-8 activation. Cell Death Differ. 2013;20(7):878-87.
49. Young TM, Reyes C, Pasnikowski E, Castanaro C, Wong C, Decker CE, et al. Autophagy protects tumors from T cell-mediated cytotoxicity via inhibition of TNFα-induced apoptosis. Sci Immunol. 2020;5(54):eabb9561.
50. Tsai TH, Lieu AS, Huang TY, Kwan AL, Lin CL, Hsu YC. RTA404, an Activator of Nrf2, Activates the Checkpoint Kinases and Induces Apoptosis through Intrinsic Apoptotic Pathway in Malignant Glioma. J Clin Med. 2021;10(21):4805.
51. Towers CG, Wodetzki D, Thorburn A. Autophagy and cancer: Modulation of cell death pathways and cancer cell adaptations. J Cell Biol. 2020;219(1):e201909033.
52. Mgrditchian T, Arakelian T, Paggetti J, Noman MZ, Viry E, Moussay E, et al. Targeting autophagy inhibits melanoma growth by enhancing NK cells infiltration in a CCL5-dependent manner. Proc Natl Acad Sci U S A. 2017;114(44):E9271-E9279.
53. Harlin H, Meng Y, Peterson AC, Zha Y, Tretiakova M, Slingluff C, et al. Chemokine expression in melanoma metastases associated with CD8+ T-cell recruitment. Cancer Res. 2009;69(7):3077-85.
54. Clancy-Thompson E, Perekslis TJ, Croteau W, Alexander MP, Chabanet TB, Turk MJ, et al. Melanoma Induces, and Adenosine Suppresses, CXCR3-Cognate Chemokine Production and T-cell Infiltration of Lungs Bearing Metastatic-like Disease. Cancer Immunol Res. 2015;3(8):956-67.
55. Wei H, Guan JL. Blocking tumor growth by targeting autophagy and SQSTM1 in vivo. Autophagy. 2015;11(5):854-5.
56. Poillet-Perez L, Xie X, Zhan L, Yang Y, Sharp DW, Hu ZS, et al. Autophagy maintains tumour growth through circulating arginine. Nature. 2018;563(7732):569-573.
57. Amaravadi RK, Kimmelman AC, Debnath J. Targeting Autophagy in Cancer: Recent Advances and Future Directions. Cancer Discov. 2019;9(9):1167-1181.
58. Arnold R, Vehns E, Randl H, Djabali K. Baricitinib, a JAK-STAT Inhibitor, Reduces the Cellular Toxicity of the Farnesyltransferase Inhibitor Lonafarnib in Progeria Cells. Int J Mol Sci. 2021;22(14):7474.
59. Pua HH, Dzhagalov I, Chuck M, Mizushima N, He YW. A critical role for the autophagy gene Atg5 in T cell survival and proliferation. J Exp Med. 2007;204(1):25-31.

60. DeVorkin L, Pavey N, Carleton G, Comber A, Ho C, Lim J, et al. Autophagy Regulation of Metabolism Is Required for CD8(+) T Cell Anti-tumor Immunity. Cell Rep. 2019;27(2):502-513.e5.
61. Starobinets H, Ye J, Broz M, Barry K, Goldsmith J, Marsh T, et al. Anti-tumor adaptive immunity remains intact following inhibition of autophagy and antimalarial treatment. J Clin Invest. 2016;126(12):4417-4429.

SUPPORTING INFORMATION

Additional supporting information can be found online in the Supporting Information section at the end of this article.

How to cite this article: Tang L, Zhang H, Zhou F, Wei Q, Du M, Wu J, et al. Targeting autophagy overcomes cancer-intrinsic resistance to CAR-T immunotherapy in B-cell malignancies. Cancer Commun. 2024;1–25.
https://doi.org/10.1002/cac2.12525